

AD-A147 587

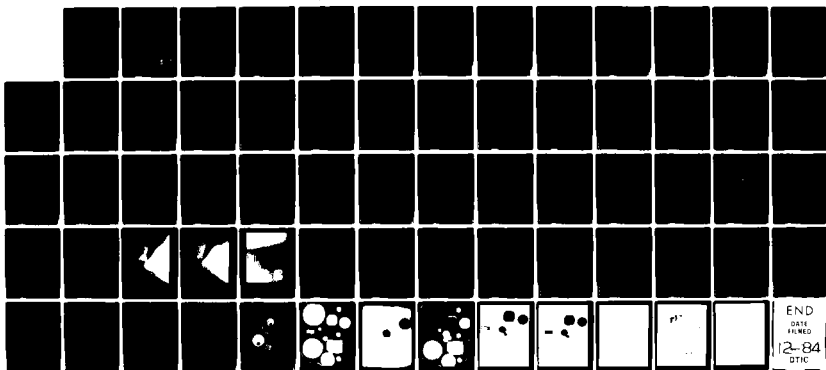
IMPROVED RADIOGRAPHIC VIEWING SYSTEM(U) CHRYSLER CORP
HUNTSVILLE AL MILITARY-PUBLIC ELECTRONIC SYSTEMS
E W GEORGE ET AL. 06 APR 84 DAMD17-83-C-3006

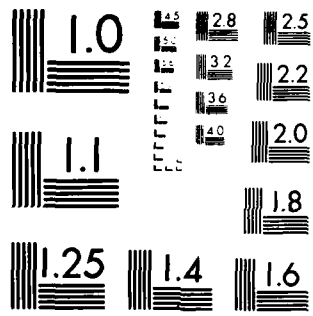
1/1

UNCLASSIFIED

F/G 6/12

NL





MICROCOPY RESOLUTION TEST CHART
NATIONAL BUREAU OF STANDARDS 1963-A

12

AD _____

IMPROVED RADIOGRAPHIC VIEWING SYSTEM

FINAL SUMMARY REPORT

(15 January, 1983 - 15 April, 1984)

E.W. George and L.M. Perry

April 6, 1984

Supported by

U.S. ARMY MEDICAL RESEARCH AND DEVELOPMENT COMMAND
Fort Detrick, Frederick, Maryland 21701-5012

Contract No. DAMD17-83-C-3006

Chrysler Corporation
Chrysler Military-Public Electronic Systems Division
Huntsville, Alabama 35805

DTIC FILE COPY

AD-A147 587

Original contains color
plates: All DTIC reproductions
will be in black and
white.

APPROVED FOR PUBLIC USE
DISTRIBUTION UNLIMITED

DTIC
ELECTE
NOV 15 1984
S A

The findings in this report are not to be construed as an official Department of the Army position unless so designated by other authorized documents.

84 11 2 091

REPORT DOCUMENTATION PAGE		READ INSTRUCTIONS BEFORE COMPLETING FORM
1. REPORT NUMBER	2. GOVT ACCESSION NO.	3. RECIPIENT'S CATALOG NUMBER
4. TITLE (and Subtitle) IMPROVED RADIOGRAPHIC VIEWING SYSTEM		5. TYPE OF REPORT & PERIOD COVERED FINAL SUMMARY REPORT 15 JAN. 1983 - 15 APR. 1984
7. AUTHOR(s) E. W. GEORGE AND L. M. PERRY		6. PERFORMING ORG. REPORT NUMBER
9. PERFORMING ORGANIZATION NAME AND ADDRESS CHRYSLER MILITARY-PUBLIC ELECTRONIC SYSTEMS 5021 BRADFORD BLVD. HUNTSVILLE, AL 35805		8. CONTRACT OR GRANT NUMBER(s) DAMD17-83-C-3006
11. CONTROLLING OFFICE NAME AND ADDRESS U. S. ARMY MEDICAL RESEARCH & DEVELOPMENT COMMAND FORT DETRICK, FREDRICK, MARYLAND 21701-5012		10. PROGRAM ELEMENT, PROJECT, TASK AREA & WORK UNIT NUMBERS 64717A.3S464717D832.BA. 024
14. MONITORING AGENCY NAME & ADDRESS (if different from Controlling Office)		12. REPORT DATE APRIL 6, 1984
		13. NUMBER OF PAGES 60
		15. SECURITY CLASS. (of this report) UNCL
		15a. DECLASSIFICATION/DOWNGRADING SCHEDULE
16. DISTRIBUTION STATEMENT (of this Report) APPROVED FOR PUBLIC RELEASE DISTRIBUTION UNLIMITED		
17. DISTRIBUTION STATEMENT (of the abstract entered in Block 20, if different from Report)		
18. SUPPLEMENTARY NOTES		
19. KEY WORDS (Continue on reverse side if necessary and identify by block number) X-Ray, Scintillator, Radiographic		
20. ABSTRACT (Continue on reverse side if necessary and identify by block number) An improved radiographic viewing system was developed for field medical X-ray applications. This effort began with research on state-of-the-art technology in X-ray to light conversion screens (especially fiber optic scintillators), image intensifiers, and detectors. The findings of this research were used to design a radiographic camera which was then constructed and tested. It is lightweight, compact, rugged, with good resolution and sensitivity.		

TABLE OF CONTENTS

<u>SECTION</u>	<u>TITLE</u>	<u>PAGE</u>
	TITLE PAGE	i
	TABLE OF CONTENTS	ii
	LIST OF ILLUSTRATIONS	iv
	LIST OF TABLES	v
	PHOTOS	vi
	SUMMARY	vii
	ABBREVIATIONS	viii
1.	INTRODUCTION	1
	1.1 History Background	1
	1.2 The Need for an Improved Radiographic System	2
	1.3 The Future of Digital Radiography	3
2.	SUMMARY OF WORK	4
	2.1 The X-ray Conversion Screen	4
	2.1.1 Material Evaluation	5
	2.1.2 Material Test Procedure	18
	2.1.3 Material Test Results	20
	2.1.4 Fiber Drawing Technology	25
	2.1.5 Construction of the FOS Conversion Screen	26
	2.1.6 Test of the FOS Conversion Screen	27
	2.2 The Image Intensifier	27
	2.2.1 Description	27
	2.2.2 Features	28
	2.3 CCD Image Detector	28
	2.3.1 Description	28
	2.3.2 Features	29
	2.4 The FOS Radiographic Viewing System	29
	2.4.1 Description of Equipment	29
	2.4.2 Performance of the FOS System	33
	2.5 Conclusions to Work Summary	33
3.	RELATED RESEARCH TOPICS	38
	3.1 Digital Image Processing	38
	3.1.1 Subtraction	38
	3.1.2 Spatial Filtering	39

TABLE OF CONTENTS (Cont'd.)

<u>SECTION</u>	<u>TITLE</u>	<u>PAGE</u>
3.1.3	Pixel Shifting	39
3.1.4	Temporal Filtering	39
3.1.5	Intensity Transformations	40
3.1.6	Parametric Imaging	40
3.1.7	Quantitative Imaging	40
3.2	Optical Data Storage (ODS)	41
4.	GENERAL CONCLUSIONS AND RECOMMANDATIONS	42
	BIBLIOGRAPHY	43
	LITERATURE CITED	49

Accession For	
NTIS GRA&I	<input checked="" type="checkbox"/>
DTIC TAB	<input type="checkbox"/>
Unannounced	<input type="checkbox"/>
Justification	
Distribution/	
Availability/	
Date of Report	
Date of Issuance	
A-1 207	



LIST OF ILLUSTRATIONS

<u>NUMBER</u>	<u>TITLE</u>	<u>PAGE</u>
2.1	X-Ray Attenuation of Phosphors vs. Energy	7
2.2	Emission Spectra of Several Common Inorganic Scintillators	8
2.3	Relative Importance of Three Major Types of Gamma Ray Interaction	12
2.4	X-Ray Attenuation in Scintillating Glas	15
2.5	Directional Distribution of Photoelectrons	16
2.6	Relative Light Output for Glass Scintillator versus Thickness for Various X-Ray Energies	19
2.7	Exposure Data of Tri-X Film for Material Testing	21
2.8	Gamma Curve for Films Used in Test	23
2.9	Scintillator Luminous Intensity versus X-Ray Source Potential ..	24
2.10	Sensor Assembly	30
2.11	Electronics Package	31
2.12	FOS System Components	32
2.13	Unprocessed Image	34
2.14	Processed Image	35
2.15	Resolution Target	36

LIST OF TABLES

<u>TABLE</u>	<u>TITLE</u>	<u>PAGE</u>
2.1	Properties of Common Inorganic Scintillators	6
2.2	Properties of Some Commercially Available Organic Scintillators	9
2.3	Absorption Coefficients of Typical X-Ray Scintillating Glass Components	14

LIST OF PHOTOS

PHOTO

All Photos in Rear Cover Pocket

- 1 Scintillating Material Sample Array at Low X-Ray Potential on Tri-X Film
- 2 Scintillating Material Sample Array at High X-Ray Potential on Tri-X film
- 3 Scintillating material Sample Array on Vericolor L Film
- 4 Scintillating Material Sample Array at Low X-Ray Potential on Vericolor L Film. Defocused
- 5 Scintillating Material Sample Array at High X-Ray Potential on Vericolor L Film. Defocused
- 6 CaF_2 (En) Stack at 12 Minute Exposure
- 7 BGO Stack at 8 Minute Exposure
- 8 Fiber Optic Scintillator (FOS) plate at 0.5 Minute Exposure

SUMMARY

The purpose of the U.S. Army Medical Research and Development Command Contract No. DAMD17-83-C-3006 was the development of an improved radiographic viewing system which would be useful in field medical X-ray applications. This effort began with research on state-of-the-art technology in X-ray to light conversion screens (especially fiber optic scintillators), image intensifiers, and detectors. The findings of this research were used to design a radiographic camera which was then constructed and tested. After construction and testing, it was found that the radiographic camera, which utilized a fiber optic scintillator (FOS) conversion screen, met all of the design criteria. It was lightweight, compact, and rugged and it had good resolution and superb sensitivity. The camera also produced digital images which allowed for digital storage, processing, and transmission of those images. It is concluded that this effort was a successful test of the technological feasibility of constructing a radiographic camera based on FOS technology. Further, it is recommended that a larger format camera be constructed, based on the same design criteria, for more thorough testing and evaluation in a medical environment.

ABBREVIATIONS

CCD	Charge Coupled Device
CRT	Cathode Ray Tube
CSH	Combat Support Hospital
CT	Computed Tomography
DSA	Digital Subtraction Angiography
EVAC	Evacuation Hospital
FOS	Fiber Optic Scintillator
MASH	Mobile Army Surgical Hospital
MPES	Military-Public Electronic Systems
MTF	Modulation Transfer Function
NMR	Nuclear Magnetic Resonance
ODS	Optical Data Storage
R&D	Research and Development
TV	Television

SECTION 1. INTRODUCTION

The purpose of the U.S. Army Medical Research and Development Command Contract No. DAMD17-83-C-3006 was the development of an improved radiographic viewing system which would be useful in field medical X-ray applications. This effort began with research on state-of-the-art technology in X-ray to light conversion screens, image intensifiers, and detectors. The findings of this research were used to design a radiographic camera which was then constructed and tested.

1.1 Historical Background

Both radiography and fluoroscopy have steadfast traditions. One of these traditions is that radiographs must be made on photosensitive film. Another idea is that the only source of fluoroscopic images are those obtained through an image intensifier tube. Radiology has been treated in the past as a film procedure, however, present day technology in processing and electronic recording techniques is rapidly replacing these older methods.

During the first sixty years of radiography and fluoroscopy research, the improvements in X-ray technology have consisted of refinements to X-ray tube power output, film processing automation and general equipment packaging with little attention toward better quality images. In the last fifteen years, X-ray technology has changed dramatically. For example, computer processing of image data has introduced digital radiography and computed tomography (CT). Fiber optics technology has improved coupling between image intensifiers and television cameras. Colorgraphic imagery has made it possible for the radiologists to more accurately analyze X-ray film. Also, electronic printers make archival-quality permanent records.

In conventional radiography, the use of film as a recording medium is difficult to replace with electronic equipment. Film is very sensitive to light, equally usable over large areas, and has good resolution and contrast. These characteristics make film a strong competitor. Considering the equipment investment and labor, radiography is a reasonable cost alternative to all-electronic processing and recording for civilian application. With the use of intensifying screens and energy filtering processes, radiography has become highly refined. However, the process is not without imperfections. Film development is messy and sensitive to temperature changes, which makes

the process very difficult to use in a field military environment. For legal and medical reasons, film must be kept for a period of several years. The storage of films generates several problems:

- a. A great deal of space is occupied;
- b. The weight of a large number of films is considerable;
- c. The filing and retrieval from files requires a great deal of labor;
- d. Storage is expensive in that the films must be adequately secure from accidental destruction;
- e. Stored film is a serious fire hazard.

Several organizations are currently developing radiographic systems, viewing stations, and storage files that are completely digital and electronic. In this way, film processing and storage is eliminated and replaced by magnetic or, more recently, optical storage of digital images. Digital radiography also permits interactive image processing for image enhancement and the transmission of digital images over standard computer communications lines for consultations.

1.2 The Need for an Improved Radiographic System

With recent technological advances, it is feasible to construct a radiographic system which has the following attributes:

- a. Lightweight;
- b. More compact;
- c. More solid-state;
- d. Greater sensitivity and resolution than current systems;
- e. Produces digital images.

For military field applications, these attributes translate into the following:

- a. Greater portability;
- b. More rugged;
- c. Lower patient X-ray dose;
- d. Image enhancement capability;
- e. Elimination of film processing, handling, and storage;

- f. More modes of operation from a single unit (digital radiography, digital fluoroscopy, and computed tomography);
- g. Image transmission capability.

All the above capabilities would be greatly beneficial in such facilities as the Mobile Army Surgical Hospital (MASH), the Combat Support Hospital (CSH), and the Evacuation Hospital (EVAC). Furthermore, such a system would fill a gap in the private sector which is currently seeing a drive toward full digitization of radiological facilities. This system could provide the means for producing digital radiographic images to replace those images currently made on film and would be more compatible with the newer digital techniques of CT, nuclear magnetic resonance (NMR), Nuclear Medicine, and Digital Fluoroscopy.

1.3 The Future of Digital Radiography

It seems to be the consensus that the evolution of digital radiography will lead to the integration of digital imaging technology throughout the radiology department and the hospital. The digital department concept has as its goal more efficient access to radiologic images from all sources (including X-ray, CT, ultrasound, NMR, etc.) for primary interpretation as well as consultation and reference. In addition to more efficient access, digital imaging will allow computer image processing which will enhance selected attributes of an image as an aid to interpretation (See Section 3.1).

The technological developments necessary for the implementation of a fully digital radiographic department are currently being researched by many people. Evidence for this lies in the many papers and presentations submitted at the Second International Conference and Workshop on Picture Archiving and Communication Systems (PACS II) for Medical Applications held in Kansas City in May 1983. Current research addresses such topics as the following: communication networks and standards; archival storage (see Section 3.2); display systems and requirements; and data compression. Fault tolerant computers necessary for this application have been developed, such as Tandem and Stratos computers. A digital sensor to replace X-ray film, being researched in this effort, utilizes fiber optic scintillator (FOS) technology to produce a high-quality, state-of-the-art digital X-ray sensor. Thus, the X-ray camera being developed under this contract is viewed as an important technological contribution in the realization of the completely digital radiology department.

SECTION 2. SUMMARY OF WORK

The work done in fulfillment of Phase I of the development of an improved radiographic viewing system is described in this section. The effort began with research on the state-of-the-art technology in X-ray conversion screens, image intensifiers, and detectors. Tests were conducted on several conversion screen materials and a fiber optic scintillator (FOS) conversion screen was manufactured. A radiographic camera was designed by coupling the FOS conversion screen with a second generation image intensifier and a two-dimensional charge coupled device (CCD) detector. The radiographic camera was then constructed and tested.

2.1 The X-ray Conversion Screen

The conversion screen is the element that converts X-ray energy (X-ray photons) into light energy or light photons. This is accomplished in a thin film of a scintillator or phosphor material. There is an unfortunate paradox in conversion screens. If the screen is thin enough to give the resolving power required, the sensitivity is typically very low, however, if the screen is thick enough to give adequate sensitivity, the resolution is inferior. The fiber optics scintillator (FOS) is the first approach that is able to circumvent this problem. In a fiber optic scintillator, light is channeled by fine fibers of a scintillating glass material, making a thick phosphor and, at the same time, maintaining high resolution and contrast. Various materials have been developed for conventional X-ray screens. The gadolinium oxysulfide and lanthanum oxysulfide screens are considered to be the most sensitive. The sensor spectral sensitivity must be considered in the evaluation of a conversion screen's spectral output. Typical phosphor screens produce a blue or green image but some screens have been produced with outputs in red and yellow. Efficiency is best accomplished if spectral output of the FOS conversion screen matches the peak sensitivity of the image intensifier and/or image sensor. Major improvements in conversion screens can be accomplished when more efficient glass scintillator materials are developed. Typical glass scintillators are presently in the 10% quantum efficiency category while the very best materials are around 50% efficient.

2.1.1 Material Evaluation. The parameters that influence the performance of an X-ray scintillator¹⁻⁴, particularly a fiber optic scintillator, are addressed in this section. A useful scintillator for X-rays should possess several characteristics:

- a. Convert the radiation into light with a high scintillation efficiency;
- b. Be transparent to the light emitted to provide good light collection; and
- c. Exhibit a short decay time.

A fiber optic scintillator should have these qualities and in most cases should have an index of refraction (approximately 1.5) so that the light can be coupled into glass fibers or image intensifier or camera tubes. The scintillator should possess good optical properties, be capable of being fabricated in small diameter fibers and be capable of being coated or graded to maintain good internal reflection of the light generated.

There are many categories of X-ray scintillator materials. A common division is organic and inorganic. The most widely used scintillators are inorganics such as ZnS, NaI, CsI and others. Properties of several inorganic scintillator materials⁴ are given in Table 2.1. A common material⁵ not included in this tabular listing is calcium tungstate, CaWO₄ (density 6.1 g/cc; decay time 10 μ s; peak of spectral emission about 430 nm). Also not included in Table I are the widely used rare earth phosphors,⁶ gadolinium and lanthanum oxysulfides. These phosphors emit in the blue, blue-green spectral region upon X-ray excitation and exhibit good X-ray attenuation in the medical X-ray energy range, as shown in Figure 2.1. Additional spectral emission information for common inorganic scintillators⁴ is given in Figure 2.2, along with the response of widely used photocathodes.

Organic phosphors such as anthracene and stilbene have been used for many years. A number of plastic and liquid scintillators are now commercially available.⁴ Table 2.2 outlines the properties of many useful organic scintillators.

The inorganic phosphors tend to have the best light output but show relatively slow response. Organic scintillators give very fast response but generally yield less light.

Table 2.1. Properties of Common Inorganic Scintillators

Material	Wavelength of Maximum Emission (nm) λ_m	Decay Constant (μs)	Index of Refraction at λ_m	Specific Gravity	γ Scintillation Efficiency Relative to NaI(Tl)	Ref.
NaI(Tl)	410	0.23	1.85	3.67	100%	A
CsI(Na)	420	0.63	1.84	4.51	85	A
CsI(Tl)	565	1.0	1.80	4.51	45	A
$^6\text{LiI}(\text{Eu})$	470-485	1.4	1.96	4.08	35	A
ZnS(Ag) ^a	450	0.20	2.36	4.09	130 ^b	B
CaF ₂ (Eu)	435	0.9	1.44	3.19	50	A
Bi ₄ Ge ₃ O ₁₂	480	0.30	2.15	7.13	8	A
CsF	390	0.005	1.48	4.11	5	A
Li glass ^c	395	0.075	1.55	2.5	10	B

^aPolycrystalline.

^bFor alpha particles.

^cTypical properties vary with exact formulation.

A. Scintillation Phosphor Catalog, The Harshaw Chemical Company.

B. Table of Physical Constants of Scintillators, Nuclear Enterprises, Inc.

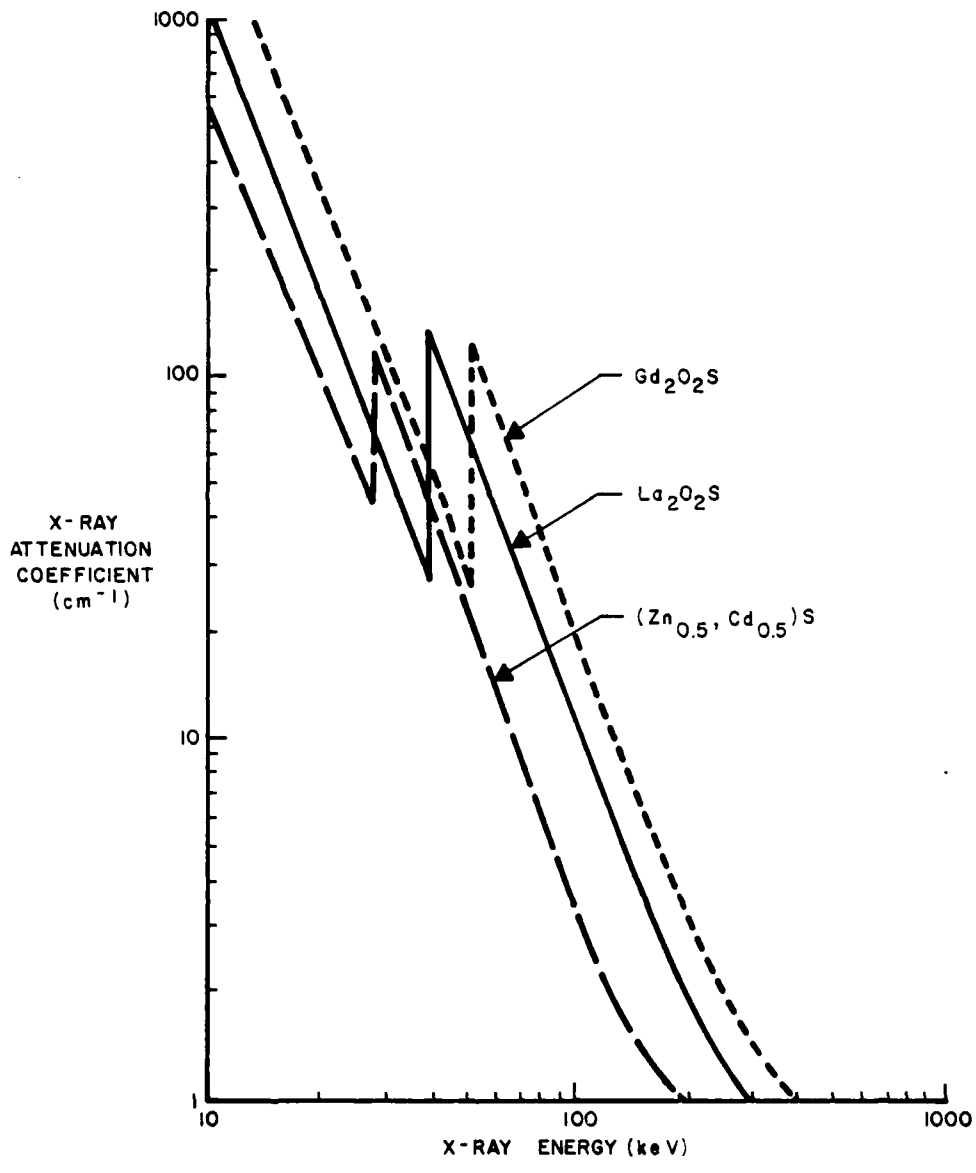
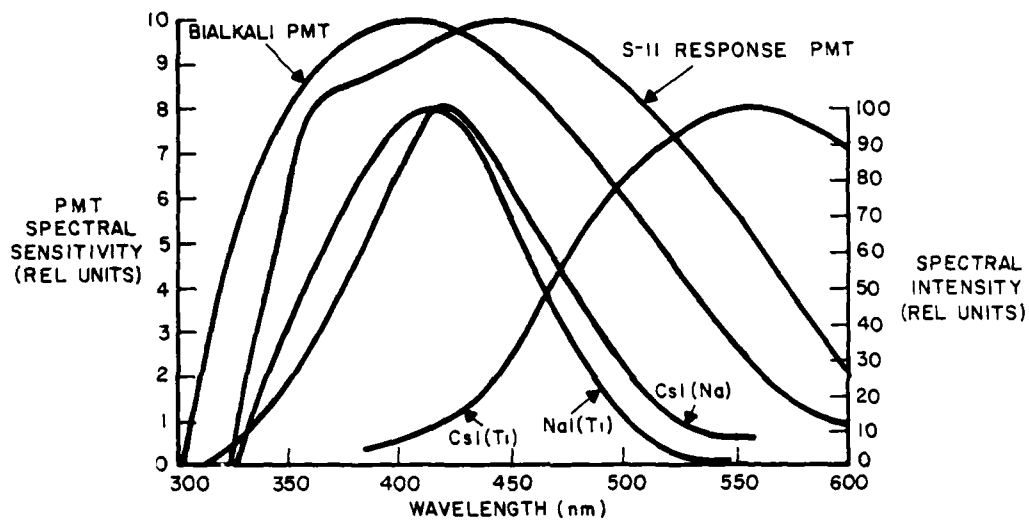


Figure 2.1. X-Ray Attenuation of Phosphors vs. Energy. See Reference 6.



The emission spectra of several common inorganic scintillators. Also shown are the response curves for two widely used photocathodes. (From Scintillation Phosphor Catalog, The Harshaw Chemical Company.) See Reference 4, page 257.

Figure 2.2. Emission Spectra of Several Common Inorganic Scintillators

Table 2.2. Properties of Some Commercially Available Organic Scintillators

Crystal	Scintillator	Type	Density	Refractive Index	Melting Softening or Boiling Point ^{°C}	Light Output & Antiscatter ^a	Decay Constant Main Component, ns	Wave-length of Maximum Emission nm	Content of Loading Element, % by Wt.	H/C No. of H Atoms/ No. of C Atoms	Principal Applications ^b
Crystal	Anthracene	Crystal	1.25	1.62	217	100	30	447		0.715	γ , α , β , fast n
	Stilbene	Crystal	1.16	1.626	125	50	4.5	410		0.858	fast n (P.S.D.), γ , etc.
Plastic	NE 102	Plastic	1.032	1.581	75	65	2.4	423		1.104	γ , α , β , fast n dosimetry
	NE 110	Plastic	1.037	1.58	75	46	~2.4	423		1.104	γ , α , β , fast n, etc.
	NE 111	Plastic	1.032	1.58	75	55	1.7	375		1.096	Ultra-fast timing
	NE 113	Plastic	1.032	1.58	75	60	3.3	434		1.108	Solvent bondable
	NE 140	Plastic	1.045	1.58	75	58	~2	425	Sn 5%	1.100	Fast counting
	Pilot B	Plastic	1.032	1.58	75	68	1.8	408		1.104	Fast n, protons, electrons
	Pilot F	Plastic	1.032	1.58	75	64	2.1	425		1.100	Ultra-fast timing
	Pilot U	Plastic	1.032	1.58	75	67	1.36	391		1.102	Fast n, protons, electrons, large area applications
	Pilot Y	Plastic	1.032	1.58	75	60	3.1	432			
Liquid	NE 213	Liquid	0.874	1.508	141	78	3.7	425		1.213	fast n (P.S.D.)
	NE 216	Liquid	0.885	1.523	141	78	3.5	425		1.171	α , β (internal counting)
	NE 220	Liquid	1.036	1.442	104	65	3.8	425		1.069	α , β (internal aqueous sample)
	NE 221	Gel	1.08	1.442	104	55	4	425		1.069	α , β (internal counting)
	NE 224	Liquid	0.877	1.505	169	80	2.6	425		1.130	γ , fast n
	NE 226	Liquid	1.61	1.38	80	20	3.3	430		0	γ , insensitive to n
	NE 228	Liquid	0.735	1.403	99	45	3.0	385	D 14.2%	2.00	(D/C) special applications
	NE 230	Deuterated Liquid	0.945	1.50	81	60	3.0	425		0.984	special applications
	NE 231	Liquid	0.88	1.50	80	58	2.8	425	D 24.5%	0.984	special applications
	NE 232	Deuterated Liquid	0.89	1.43	81	60	4	430		1.96	(D/C) special applications
Loaded	NE 233	Liquid	0.874	1.506	117	74	3.7	425		1.118	α , β (internal counting)
	NE 235A (235H)	Liquid	0.858	1.47	350	40(50)	4	420		2.0	α , fast n, large tanks
	NE 250	Liquid	1.035	1.452	104	50	4	425		1.760	α , β (internal, aqueous sample)
	NE 260	Liquid				40		425			α , β (internal counting)
Liquid	NE 311	B ¹⁰ Loaded	0.91	1.411	85	65	3.8	425	B 5%	1.701	n, β
	(311A)										
	NE 313	Gd Loaded	0.88	1.506	136	62	4.0	425	Gd 0.5%	1.220	n
	NE 316	Sn Loaded	0.93	1.496	148.5	35	4.0	425	Sn 10%	1.411	γ , X-rays
	NE 323	Gd Loaded	0.879	1.50	161	60	3.8	425	Gd 0.5%	1.377	n

From Table of Physical Constants of Scintillators, Nuclear Enterprises, Inc.

^aNa (Tl) is 230 percent on this scale.

^bP.S.D. represents neutron-gamma pulse shape discrimination. (See Ref. 4, pages 246-7).

For X-ray detection, many inorganic scintillators contain high Z materials and therefore show relatively good X-ray absorption. The organic materials, on the other hand, are generally low Z materials so X-ray absorption tends to be less.

For the specific application of a fiber optic scintillator one could consider inorganic scintillators in powder or crystal form. Actual fabrication of a fiber optic screen appears challenging except perhaps for special cases such as CsI which can be grown in a columnar orientation which at least simulates a fiber optic scintillator approach. The plastic scintillators can be fabricated in fiber form and assembled into an area detector. However, attempts to improve the detection efficiency of plastic scintillators by adding high Z materials have met with only limited success. It has proven difficult to find high Z compounds that are compatible with the complex plastic matrix and that can be polymerized.

The most promising class of material to consider for a fiber optic scintillator is glass; the remainder of this discussion will concern glass. However, many of the general concepts discussed, including X-ray absorption, Compton scatter, electron range, etc., apply to the other scintillator materials, as well.

A scintillator for X-rays may be thought of as a three-part material. There is a host material. In our present consideration, this is a glass. There should be a high Z material involved in order to increase the X-ray absorption. Finally, there should be a luminescence activator to control light emission. There is strong interplay between these three areas that combine to make an X-ray scintillator.

Glass scintillators normally contain about 50-60% SiO_2 . The high Z loading is usually provided in the form of PbO_2 . Ideally, one wants to load as much lead as possible into the glass to increase its density and its X-ray absorption. Loadings of PbO_2 in the order of 18% by weight are used in X-ray scintillating glasses. The lead tends to precipitate out for loadings beyond that value. This results in a glass density of 3 to 4 gm/cc.

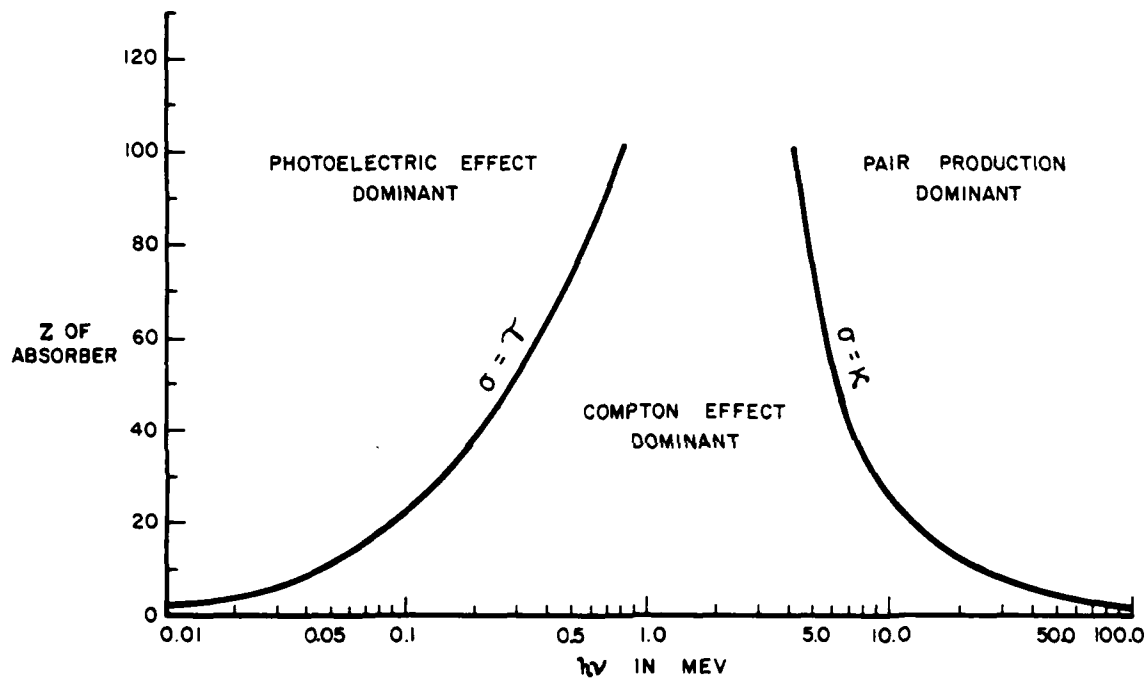
Typical luminescence activators in glass scintillators ^{7,8} are Ce^{3+} , Tb^{3+} and UO_6^{6+} . These activators provide light outputs in different spectral regions and also show different response times. Cerium activated scintillators usually emit in the near ultraviolet portion of the spectrum, 380 to

400 nm; response time is in 60-80 ns time range. Terbium activated scintillators usually emit in the 500 to 600 nm region and UO activation usually produces a yellow emission at about 580 nm; both activators yield longer response time than cerium activated scintillators. Much work has been done with cerium activation. The light output of a typical scintillating glass increases with increasing cerium content to values in the order of 4 to 6 weight percent Ce_2O_3 . The light output tends to saturate for further additions of cerium activator.

Once a fiber optic scintillator is chosen it may be sized for a particular application based on a number of factors. The first item to consider is X-ray absorption. Ideally one wants absorption close to 100% in the length of fiber for the X-ray energy under consideration. Further, it is desirable that the absorption mechanism be in a form that will stimulate emission from the luminescence activated fiber and such that the secondary radiation produced will remain in the detection fiber. The predominant absorption mechanisms⁹ are the photoelectric effect, Compton effect and pair production. In the photoelectric effect, the X-ray photon is absorbed; its energy is transferred to an electron which is ejected from an atom with sufficient energy to conserve momentum. In Compton scattering, the photon ejects an electron but does not transfer all its energy; the output is an electron and a reduced energy photon. Pair production occurs only for photons which have an energy in excess of 1.02 MeV. The photon disappears and an electron-positron pair is created.

These absorption mechanisms tend to predominate in certain energy regions, as shown in Figure 2.3. For absorbing materials with Z greater than about 20, the photoelectric effect is the primary absorption mechanism up to X-ray energies of about 100 keV. For absorbing material with a Z of about 50, the photoelectric is the dominant absorption mechanism for X-ray energies up to 300 keV.

Therefore, for a medical diagnostic system, the photoelectric effect will be the major absorption mechanism for detection. This is fortunate because the electron produced will stimulate the emission of light. Further, the range of the charged electron will not be so great as to cause significant problems with cross talk between fibers. Compton scatter and pair production, on the other hand, yield radiation that would be expected to cause cross talk between fibers.



Relative importance of the three major types of X-ray interaction. The lines show the values of Z and $h\nu$ for which the two neighboring effects are just equal. See Reference 9, page 712.

Figure 2.3. Relative Importance of Three Major Types of Gamma Ray Interaction

The absorption of the X-rays can be readily calculated from the familiar absorption equation:

$$I = I_0 e^{-ux} \quad (\text{Eqn. 2.1})$$

where I_0 is the X-ray intensity incident on a material of thickness x , having a linear absorption coefficient, u , and I is the transmitted X-ray intensity.

The value of u is energy dependent. The value of u for a compound takes into account the various components of the compound in proportion. For a typical X-ray glass scintillator for example,

$$u_{\text{Total}} = 55\% u_{\text{SiO}_2} + 18\% u_{\text{PbO}_2} + 5\% u_{\text{Ce}_2\text{O}_3} + 22\% u_{\text{Al}_2\text{O}_3} \quad (\text{Eqn. 2.2})$$

Table 2.3 lists the linear absorption coefficients for these materials for several X-ray energies of interest in the medical diagnostic range. It can be seen that the value of u is much higher for the additives (PbO_2 and Ce_2O_3) than for the glass matrix materials. Therefore, the additives control the X-ray absorption. Since the absorption takes place in these higher Z materials, it is clear from Figure 2.3 that the photoelectric effect is the main absorption mechanism for the medical diagnostic X-ray energy range. In Figure 2.4, the absorption of this typical glass (see Eqn. 2.2) is plotted as a function of X-ray energy for several different glass thicknesses. It is noted that a glass thickness of 1 cm is almost totally absorbing to X-ray energies as high as 150 keV.

It is appropriate to further examine the electrons ejected in the photoelectric process. Studies of the angle at which the electron is released have shown a dependence with X-ray energy. For high X-ray energies the electron is mostly forward directed (emitted in the same direction as the incident X-ray photon). At energies in the medical diagnostic range, the predominant angle of emission for the photoelectron is about 45° . This is shown in Figure 2.5.

It is also known that about 80% of photoelectron absorption takes place in the K shell of the atom.¹⁰ This permits us to calculate the energy of the released electron since the maximum electron energy, E_e , will be:

Table 2.3. Absorption Coefficients of Typical X-Ray Scintillating Glass Components

Photon Energy keV	SiO ₂	PbO ₂	μ (cm ⁻¹) Ce ₂ O ₃	Al ₂ O ₃
50	0.318	6.86	13.93	0.292
100	0.619	4.84	2.08	0.163
150	0.140	1.74	0.74	0.137

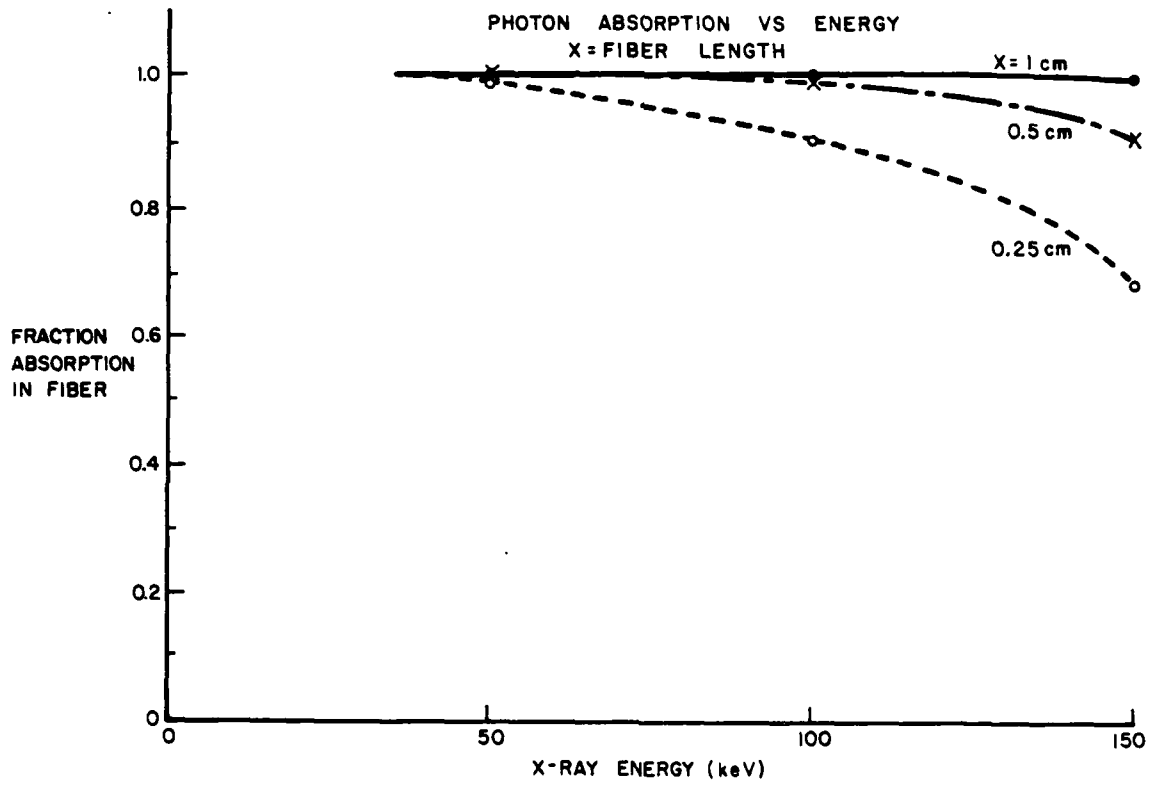
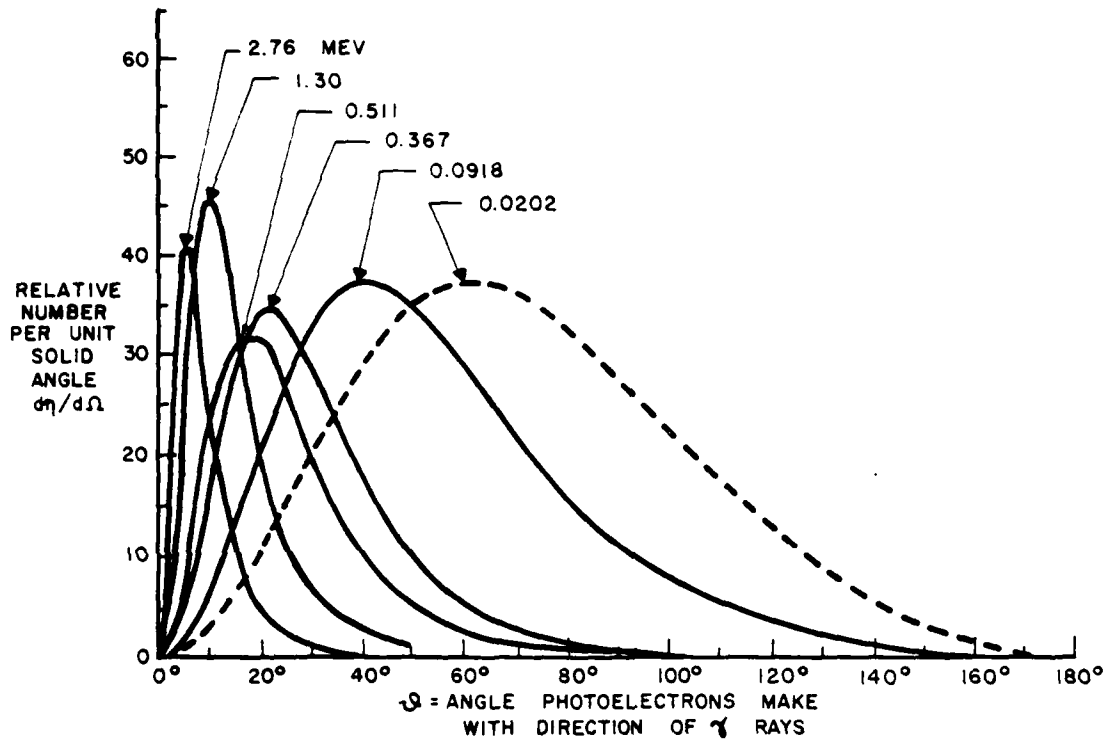


Figure 2.4. X-Ray Attenuation in Scintillating Glass



Directional distribution of photoelectrons per unit solid angle, for energies as marked. The curves are not normalized with respect to each other. See Reference 9, page 696.

Figure 2.5. Directional Distribution of Photoelectrons

$$E_e = E_p - E_B \quad (\text{Eqn. 2.3})$$

where E_p = energy of the incident photon and E_B = binding energy of the electron (assumed to be the K shell).

It has been shown that most of the absorption in an X-ray scintillating glass will take place in the Pb or Ce atoms. The binding energies for the K-shell electrons are about 88 keV for lead and about 40 keV for cerium. Therefore, in the medical diagnostic range, the emitted photoelectron will have an energy of less than 100 keV in most cases.

The range of the emitted electron can be calculated. Glocker,¹¹ for example, gives the following equation:

$$R = 4.9 (10^{-6}) E^{1.72} \quad (\text{Eqn. 2.4})$$

where R is the range of the electron in g/cm^2 and E is the electron energy in keV.

For a typical glass having a density of about 4, a 40 keV electron (as might be emitted for a 128 keV photon absorbed in the lead K shell, for example), will have range of about 7 μm . Recognizing that it comes off at an angle (see Figure 2.5), the actual radius of glass fiber needed to contain such an electron would be about 6 μm or a glass fiber diameter of 12 μm .

Calculations such as this permit one to determine the fiber diameter needed to absorb an X-ray photoelectron. The calculation assumes that the absorbing event takes place in the center of the fiber, that the electron is emitted at the full energy (this would not be the case because the X-ray beam will have a spectrum; there will be relatively few photons at the peak energy) and that the electron does not recombine before it stimulates a luminescence center. Overall, the fiber diameter so calculated tends to be conservative.

There are several factors that must be considered to determine relationships for specific scintillators in terms of light output as functions of the scintillator geometry, X-ray energy, reabsorption, light self-absorption, etc. One factor is the photofraction,¹² in effect the percentage of the total X-ray photon input converted into detectable light as a function of detector type and geometry. For most luminescence materials, the photofraction is on

the order of 80- 100% for lower energy X-rays (in the medical diagnostic range). Therefore, the light output will tend to vary primarily with the X-ray absorption - as already calculated and shown for a specific glass scintillator (Eqn. 2.2 and Figure 2.4). A plot of relative light output versus thickness for this glass is given in Figure 2.6. The light output value is arbitrarily shown as 100 for an X-ray energy of 150 kV. For lower energy X-rays, the peak light output occurs for a smaller thickness of glass scintillator because the lower energy X-rays are more readily absorbed. The relative light output for the lower X-ray energies is reduced, however, because there is less energy available to create ion pairs, which in turn leads to light stimulation. The relative values were calculated based on the X-ray energy for maximum intensity (about 2/3 the peak X-ray energy values shown in Figure 2.6).

For a nontransparent phosphor, such as a reasonably thick (approximately 0.2 mm) granular screen of zinc sulfide, calcium tungstate or gadolinium oxysulfide, the curves in Figure 2.6 would show a decrease in light output as screen thicknesses increased; some scintillations stimulated at the X-ray source side of the phosphor screen would be attenuated by scatter between the grains or by absorption within the grains. For the transparent scintillators such as glass, one must normally deal with lengths approaching a meter before light attenuation becomes of concern.

2.1.2 Material Test Procedure. All available samples of scintillating materials were mounted into a single plane matrix. This allowed all samples to be in direct contact with a sheet of 4 x 5 inch photographic film. The materials mounted for testing were the following:

1. Anthracene $C_{14}H_{10}$ - A 42 mm diameter by 14 mm thick sample of the organic crystal dispersed in a transparent castable plastic resin.
2. UV phosphor - a 35 mm diameter by 14 mm thick sample of an unknown UV phosphor dispersed in 2 mm tubes (straws) filled with plastic resin.
3. Bismuth Germanate $Bi_4Ge_3O_{12}$ - An 18 mm diameter by 18 mm thick fiber optic stack composed of 1 mm square BGO fibers.
- 4a. Calcium Fluoride $CaF_2(Eu)$ - A 12.5 mm diameter by 12 mm long sample of the inorganic crystal doped with Europium.
- 4b. Calcium Fluoride $CaF_2(Eu)$ - An 8 mm diameter by 18 mm long sample of the same material to study the effects of lengths on output light energy.

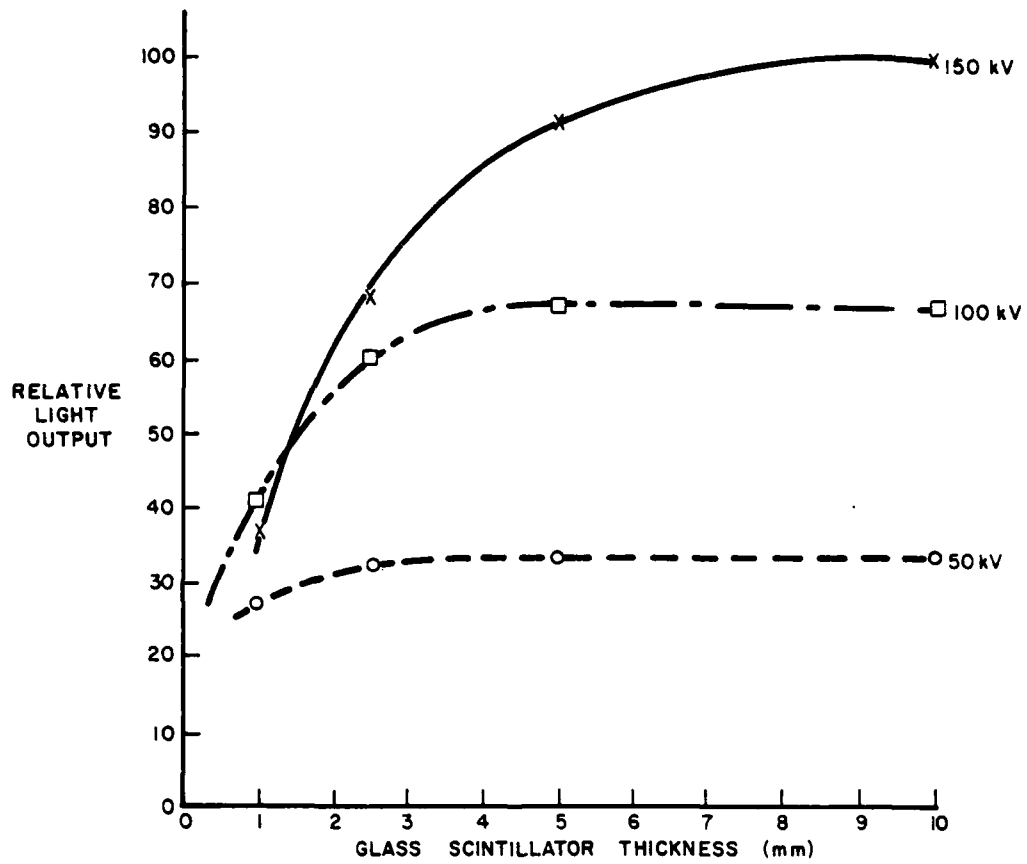


Figure 2.6. Relative Light Output for Glass Scintillator versus Thickness for Various X-ray Energies.

- 4c. Calcium Fluoride $\text{CaF}_2(\text{Eu})$ - A 10 mm x 15 mm stack of 1 mm square by 16 mm long fibers machined from calcium fluoride crystals.
5. Cerium Scintillating Glass I - A 10 mm diameter by 10 mm long sample of cerium doped phosphate glass manufactured by Kigre, Inc. and coded P423.
6. Europium - Terbium Scintillating Glass - A 10 mm diameter by 10 mm long sample of rare earth doped phosphate glass manufactured by Kigre, Inc. and coded P421.
7. Samarium Scintillating Glass - A 10 mm diameter by 10 mm long sample of samarium doped silicate glass manufactured by Kigre, Inc. and coded KSF-5.
8. Cerium Scintillating Glass II - A 6 mm diameter by 25 mm long sample of cerium doped phosphate glass manufactured by EOTEC Corporation and coded SBLO48-SP.
9. Scintillating Glass - A 24 mm fractured piece of doped silicon/barium/lithium glass manufactured by Ohara Optical Company and coded SCG-1.
10. Sodium Iodide $\text{NaI}(\text{Th})$ - A 12.5 mm diameter by 12.5 mm long sample of the most sensitive scintillating material known. The sample is thallium doped and encased in a air/water tight cell.

A plot of X-ray source potential and exposure time was drawn (Figure 2.7) to predict exposure requirements. Samples were exposed at a variety of parameters and the film evaluated for optimum exposure. With this plot, source potential and source distance can be put together to select the proper exposure time.

2.1.3 Material Test Results. The mounted scintillating material samples were exposed to X-rays as follows:

Code	Potential	Time	Current	Distance
1	20 kVp	3.5 min.	3 mA	13 in.
2	30 kVp	54 sec.	3 mA	13 in.
3	50 kVp	12 sec.	3 mA	13 in.
4	75 kVp	3 sec.	3 mA	13 in.
5	100 kVp	1.2 sec.	3 mA	13 in.
6	140 kVp	1.0 sec.	3 mA	13 in.

The Calcium Fluoride $\text{CaF}_2(\text{Eu})$ samples fluoresce most strongly at the lower X-ray potentials (see Photo 1). None of the glass or plastic samples scintillate strong enough to be detected. The Sodium Iodide $\text{NaI}(\text{Th})$ sample is the strongest scintillator at 140 kVp (see Photo 2). The Calcium Fluoride

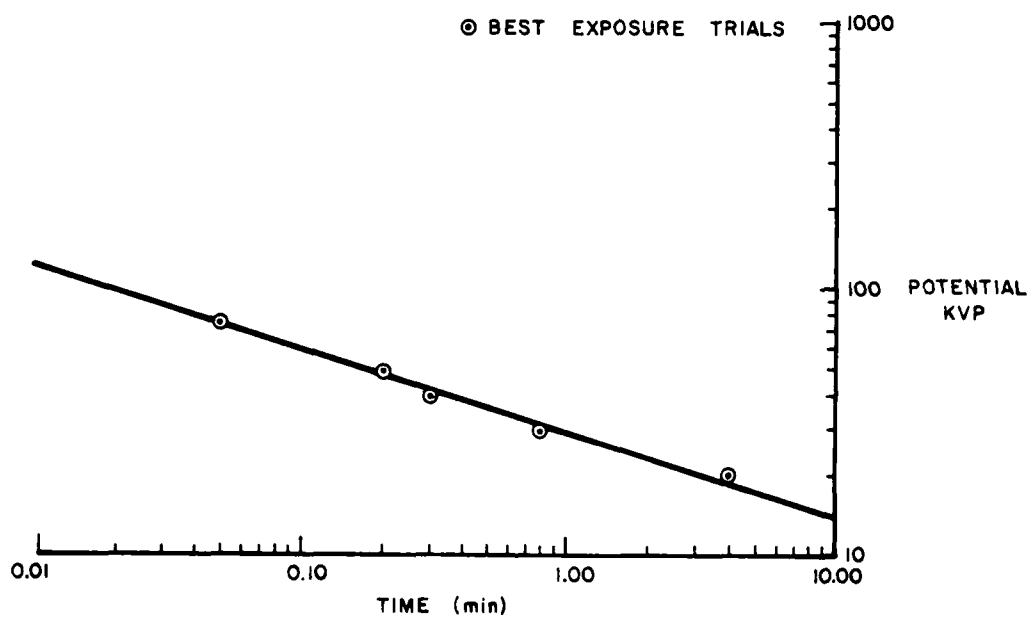


Figure 2.7 Exposure Data of Tri-X Film for Material Testing

CaF₂ (Eu) stack fluoresces at all energies. The samples were mounted in a matrix so the output surface was in contact with a sheet of Tri-X film.

The matrix of scintillating materials was exposed to X-ray radiation with another type of photographic film, Vericolor L, which is a long exposure (over 1 second) negative color film. With the use of color film, the general spectral characteristics of the scintillating radiation was observed (see Photo 3). It was found that all dopings being studied had strong emissions in the blue and violet spectrum. It was also noted that the stronger emitting materials masked the weak emissions so another test setup was designed to photograph only the direct output light.

A series of exposures were made with the scintillating material matrix on color film in a defocused configuration (see Photos 4 and 5). A piece of 2 millimeter and 5.5 millimeter plate glass was placed between the samples and an X-ray shield so only the output scintillating radiation would be recorded on film. This experiment also demonstrated the defocusing effect of a 2 millimeter faceplate separation.

The luminous intensity of all the scintillation samples described in Section 2.1.2 of an image on film is a good measure of total visible flux presented to that film. For quantitative purposes, film exposure must be kept in the straight portion of the Gamma curve. The Gamma curve (characteristic curve or contrast index curve) is a plot of film optical density versus the log to the base 10 of the exposure. The Gamma curve for the film used is shown in Figure 2.8. Film development times and temperatures must be carefully controlled for precise measurements. Stray light and direct exposure to X-rays must be minimized. By measuring the density of a scintillation image, the quantity of energy producing that image may be determined. By dividing the exposure by the time period required to produce that density, the luminous intensity of the scintillation source may be quantified. The radiant luminous intensity is the image brightness in laymen's terms. The inorganic crystal samples of NaI(Th), CaF₂(Eu) and BGO were measured at 140 kVp and their intensities plotted in Figure 2.9 with the curves of the inorganic crystals. The most important curve of course is the data on the CaF₂(Eu) crystal stack. The stack intensities are 10-15% low due to the opaque epoxy between individual crystals. The interesting point is that the crystal stack or crude

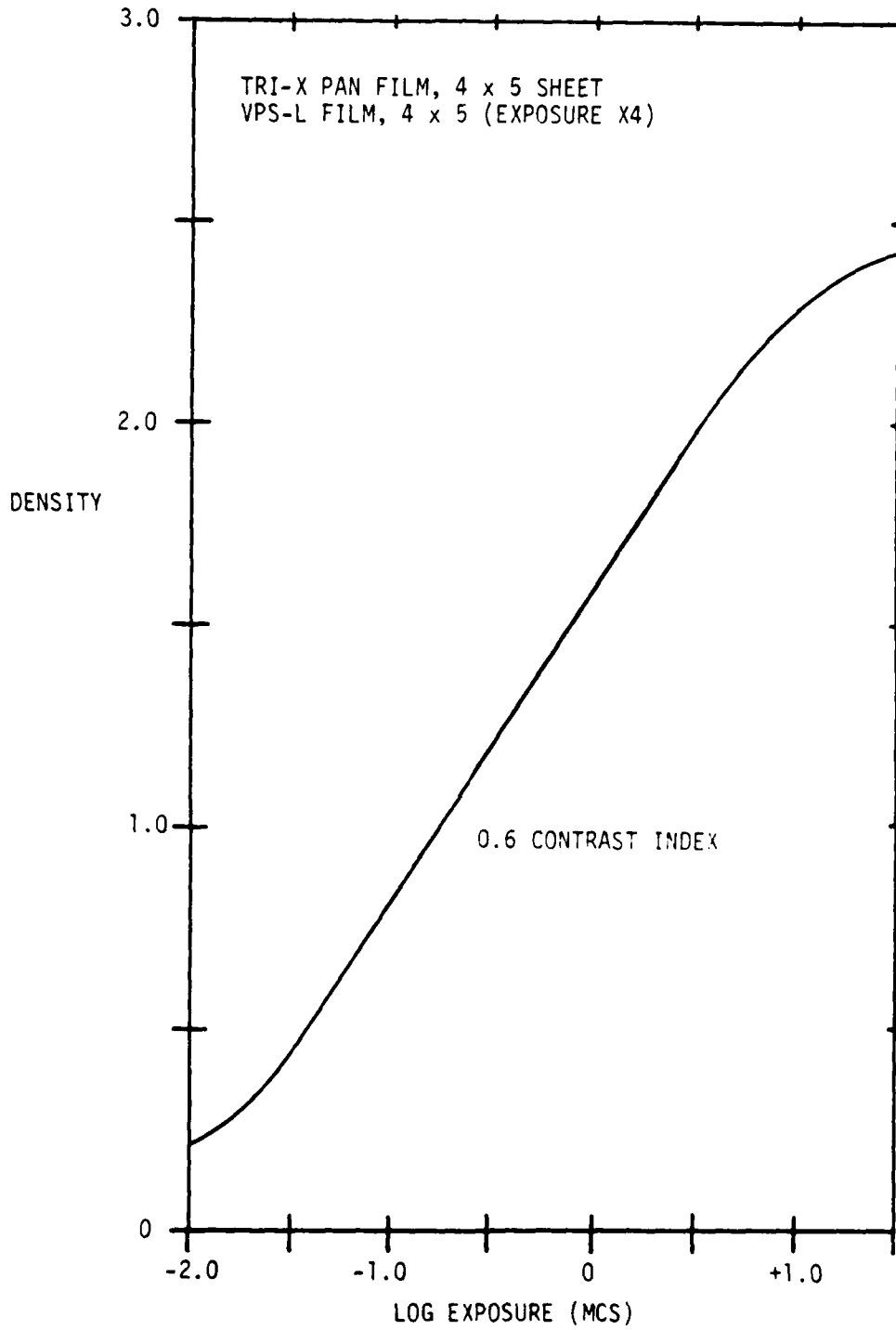


Figure 2.8. Gamma Curve for Films Used in Test

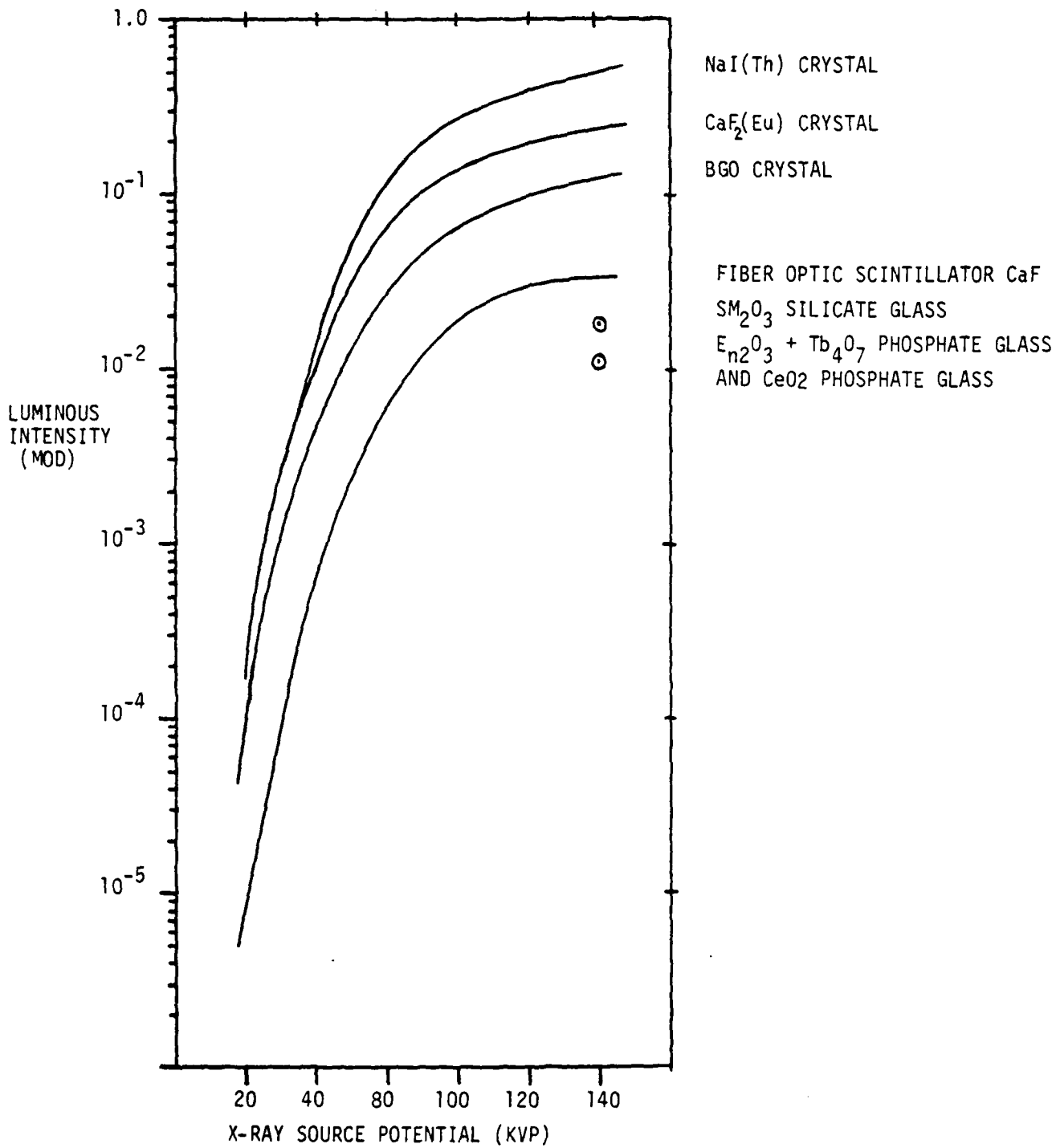


Figure 2.9. Scintillator Luminous Intensity versus X-ray Source Potential

fiber optic scintillation has a sensitivity approaching the best bulk radiation detectors and yet is capable in principle of producing a high resolution image.

2.1.4 Fiber Drawing Technology. Several methods of drawing glass into fine fibers have been developed but significant technical breakthroughs occurred in the early 1970's when fabrication of low-loss optical fiber was accomplished through doped-deposited silica technology. Very low-loss fibers require impurity levels of some transition metals of 10-50 parts per billion. Glass quality restrictions must also be controlled very tightly to limit internal scattering. The two most common versions of the doped-deposited silica process are the outside vapor-phase oxidation technique and the inside vapor-phase oxidation process. Earlier processes that can not produce very low-loss fibers include the: rod-in-tube precision drawing process, stratified melt process, and plastic spray clad technique.

The outside vapor-phase oxidation process is the process in which a fuel lean torch deposits reactants, typically SiO_4 , GeO_4 and BO_3 , on a mandrel of a glass working lathe. The metal halides react with excess oxygen at an elevated temperature in the flame to produce a stream of fine doped silica soot particles that impact on the rotating mandrel. Composition changes with successive deposited layers and is designed to yield the desired refractive index profile for core glass and cladding glass. This process allows the greatest flexibility in glass composition for both core and cladding glasses, and has resulted in cladding compositions of as high as 25% B_2O_3 for stress balancing. After enough glass has been deposited, the blank is removed from the lathe, the mandrel is removed and the blank consolidated to a dense glass preform, ready for fiber drawing.

The inside vapor-phase oxidation process starts with a high silica glass tube mounted in a glass-working lathe. Heat is applied to the outside of the glass tube by oxygen hydrogen burners while the tube is rotating. At an elevated temperature, the reactants in the tube oxidize with excess oxygen to form a fine doped silica soot on the inside surface of the glass tube. Upon subsequent heating, clear, glassy layers are formed and fused together. Reactant flow rate is changed with consecutive glass layers to control composition.

The doped-deposited silica technology of producing glass preform blanks for graded index optical fibers has maximum control over the composition and material distribution.

The actual fiber drawing technology has not changed in recent years but control mechanisms have been added to improve consistency of both optical and mechanical properties. Fibers are drawn by placing a blank of glass into a furnace, and subsequently heating the tip of the blank until the glass softens. During drawing, the core and cladding glasses maintain their respective geometric relationships, even though their diameter is drawn down by a ratio as great as 300:1. The core-to-cladding ratio and the refractive index profile of the core in the blank form are faithfully reproduced in the fiber.

2.1.5 Construction of the FOS Conversion Screen. The construction of fiber optic faceplates is somewhat different than the fabrication of low-loss optical transmission fibers. A scintillating glass is melted in a non-oxidizing furnace with a low refractive index glass floating on the surface. A glass preform is produced by drawing a 5 mm (0.20 in.) rod from the melt in a smooth continuous pull. The cladding glass is only 0.25 mm (0.01 in.) thick on the preform rod. Twenty preforms are configured into two rows of ten. All twenty preforms are drawn simultaneously into twenty 0.0158 mm (0.00062 in.) round fibers. These fibers are extended and fused together to form a flat double layer strip. After shaping and fusing a strip 0.028 mm (0.0011 in.) by 0.14 mm (0.0055 in.) is formed of approximately 0.014 mm (0.00055 in.) square fibers. Five strips or layers are fused together to form a complex fiber bundle containing 10 by 10 individual fibers. These bundles are 0.14 mm (0.0055 in.) square. A twelve by twelve stack of fiber bundles is assembled and fused together. This stack is 1.70 mm (0.067 in.) square and contains 120 by 120 fibers. A total of 14,400 fibers are in each stack. At this stage, the material looks like a one sixteenth inch clear glass rod with a square cross section. These stacks are grouped together in a 17 x 17 array to form a 28.9 mm (1.14 in.) square block of scintillating glass fibers. The block is fused together by heating to the softening point for 2 minutes and annealed. This block is sliced into various thickness plates which can be further fused together to form large area arrays. Each plate or screen is polished to a fine optical surface on both sides and one side is evaporation coated with a 0.005 mm (0.00002 in.) layer of aluminum and 0.00025 mm (0.00001 in.) layer of

SiO₂ (silicon dioxide) to form a hard quartz overcoat. After this assembly process, the fiber optic scintillating faceplate is inspected and tested.

2.1.6 Test of the FOS Conversion Screen. A fine fiber optic screen 22 x 28 millimeters (0.87 x 1.10 inches) was fabricated, sliced, and polished to 4 mm (0.16 inches) thick. The screen is a coherent fiber optic plate composed of 0.015 mm (0.0006 in.) diameter scintillating glass fibers. The screen has 67 fibers per linear millimeter which corresponds to a theoretical resolution of 33 line pairs per millimeter. The measurable resolution will be somewhat less than the theoretical value. The luminescence output of this screen material is in the yellow-green band of visible light.

To record the fluoroscopic image of luminescence energy the screen was placed on a thick slab of lead glass and photographed during exposure to X-rays. The camera and macro lens were placed in the the X-ray chamber during exposure. Three samples of fiber optic scintillators were exposed and photographed. These samples were CaF₂(Eu) (see Photo 6), BGO (see Photo 7), and the fine fiber optic scintillator screen (see Photo 8) which will be referred to as FOS. The CaF₂(Eu) crystal stack provided a brilliant blue image with a 12 minute exposure. The BGO crystal stack provided an equally bright image with 8 minutes of exposure. The luminescence was a bright green color. The FOS image was equally bright with only a 0.5 minute exposure and the luminescence a yellow-green color.

Resolution of the FOS was measured from the photographic negatives at 16 lp/mm. This is very good considering image intensifier tubes are typically 2 lp/mm and film with intensifying screens only about 4 lp/mm. This measurement also includes the MTF of the macro lens and the film, so the actual screen resolution is probably close to 20 lp/mm.

2.2 The Image Intensifier

2.2.1 Description. The Varo model 3603 is a 25 mm second generation light image intensifier with single stage electron focusing. This intensifier yields an inverted image at the output. There is a fiber optic faceplate to couple the output side with a CCD detector array. An automatic brightness control maintains an output of 5 foot lamberts by varying the gain from 10 to 10,000. The resolution of the intensifier is 1200 lines or greater over the 24 mm input diameter (greater than 25 lp/mm).

The Varo 3603 utilizes the latest technology in phosphor screens and fiber optic coupling to yield a high dynamic range of image brightness while maintaining high resolution.

2.2.2 Features

- a. Automatic brightness control to give gain of 10 to 10,000 maintaining approximately 5 foot lamberts output.
- b. Less than 20% vignetting at 24 mm.
- c. Resolution of 1200 lines or greater over 24 mm diameter.
- d. Photo-cathode with quantum efficiency of 14% or greater at 550 nm.
- e. Fiber optic input and output faceplates.
- f. Built-in converter from 3 volts dc to required internal high-voltage.
- g. 3 volt dc supply box.

2.3 CCD Image Detector

2.3.1 Description. The Fairchild CCD222 is a 488 x 380 element solid-state charge-coupled device area image sensor which is intended for use as a high-resolution detector in television compatible imaging systems and a variety of other scientific and industrial optical instrumentation systems. The CCD222 is organized as a matrix array of 488 horizontal lines by 380 vertical columns of charge-coupled photoelements. The dimensions of these 185,440 photoelements are 12 μm horizontally by 18 μm vertically. The photoelements are precisely positioned on 30 μm horizontal centers and 18 μm vertical centers. CCD222 has an active optical area of 8.8 by 11.4 mm, with a diagonal of 14.4 mm.

The low noise performance of the buried channel CCD structure provides excellent low-light-level capabilities when the sensor is cooled; performance adequate for most applications can be achieved with the sensor at room temperature or above. The geometric accuracy of the device structure, combined with a video readout which is controlled by digital clock signals, allows the signal output from each photoelement to be precisely identified for easy realization of computer-based image processing systems. The devices can be used in video cameras that require low power, small size, high sensitivity, high reliability and rugged construction.

2.3.2 Features

- a. 185,440 Sensing Elements on a Single Chip
- b. Available Horizontal Resolution : 380 Elements per Line
- c. Available Vertical Resolution: 488 Lines
- d. No Lag, No Geometric Distortion
- e. A Gamma of Unity
- f. High Dynamic Range - Typically greater than 1,000:1 at 25°C (Excluding Dark Signal Non-uniformity)
- g. Low Light Level Capability, Low Noise Equivalent Exposure
- h. Video Data Rates up to 20 MHz, Frame Rates to 90 Hz
- i. Sample-and-Hold Video Output
- j. Low Power Dissipation, Solid-State Reliability and Small Size
- k. Standard TV Aspect Ratio (4:3)
- l. Satisfies NTSC Resolution Standards
- m. Two-Phase Register Clocking
- n. Digitally-Controlled Readout

2.4 The FOS Radiographic Viewing System

2.4.1 Description of Equipment. A fiber optic scintillator (FOS) X-ray sensor has been assembled and tested. The unit consists of a sensor assembly, an interconnecting cable and a video processing electronic package. The sensor assembly is 155 mm (6.1 in.) long and 89 mm (3.5 in.) in diameter.

The sensor housing is anodized and dyed satin black. The interconnecting cable is 3.5 m (11.5 ft.) long with two connectors on each end. Figure 2.10 is a sketch of the sensor assembly. The electronic package as shown on Figure 2.11 has sufficient inputs and outputs for evaluation of fluoroscopic images. The unit is 305 mm (12 in.) by 320 mm (12.5 in.) by 110 mm (4.3 in.) tall.

The system (see Figure 2.12) is composed of a FOS conversion screen, an image intensifier and a TV camera. Two high resolution FOS screens are provided with the system. One is 2 mm thick and the other 3.6 mm thick. Both

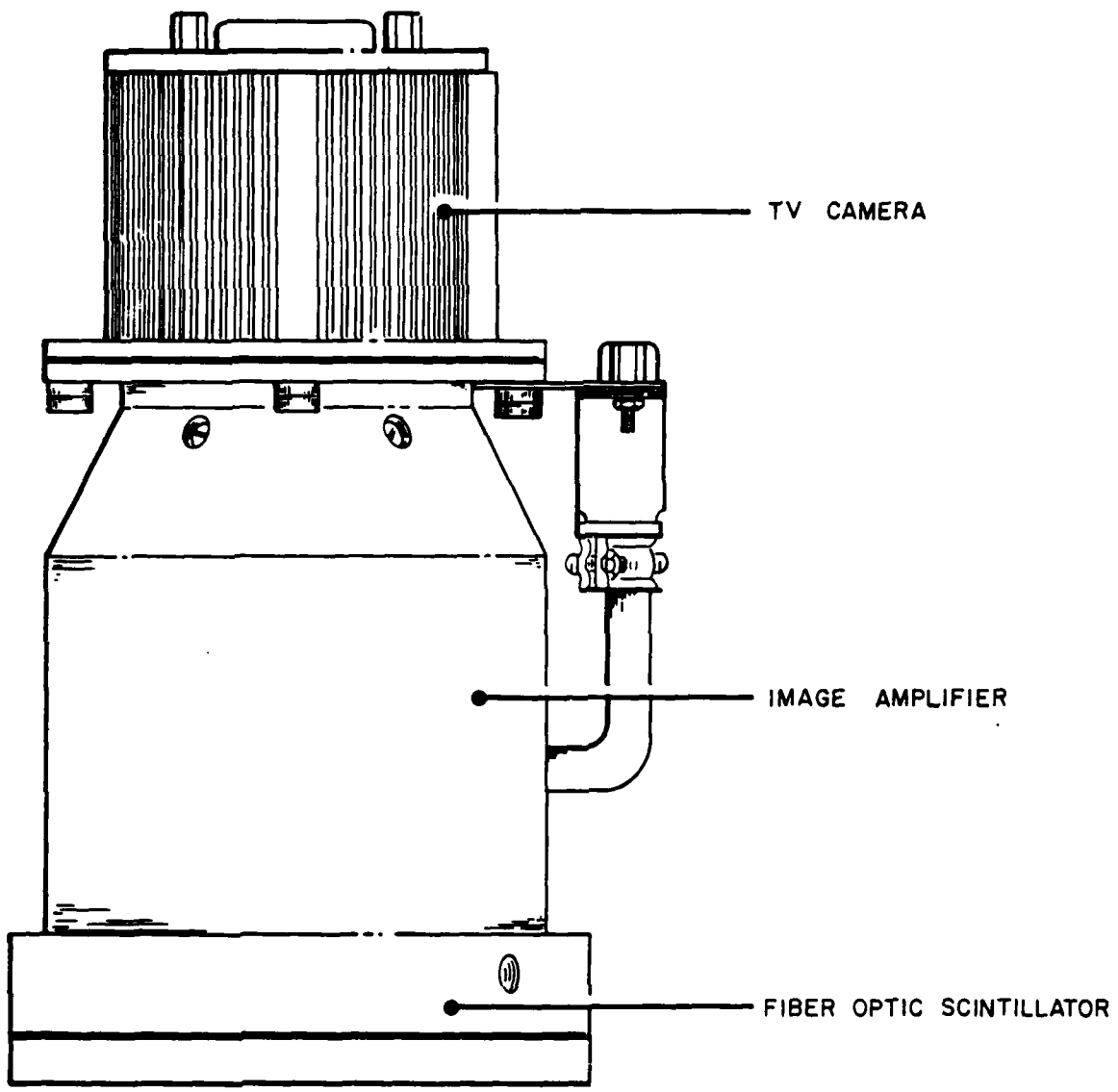


Figure 2.10. Sensor Assembly

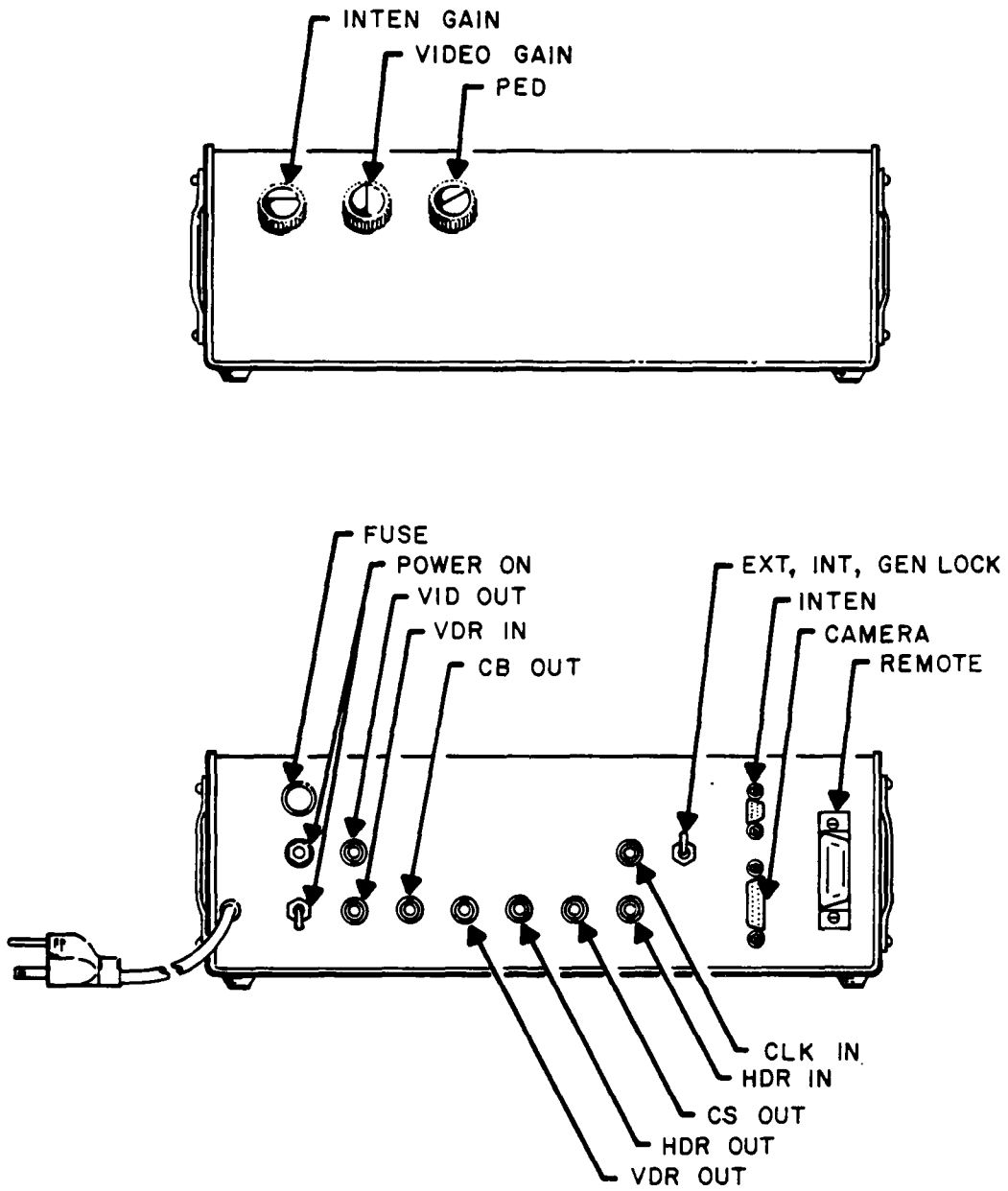
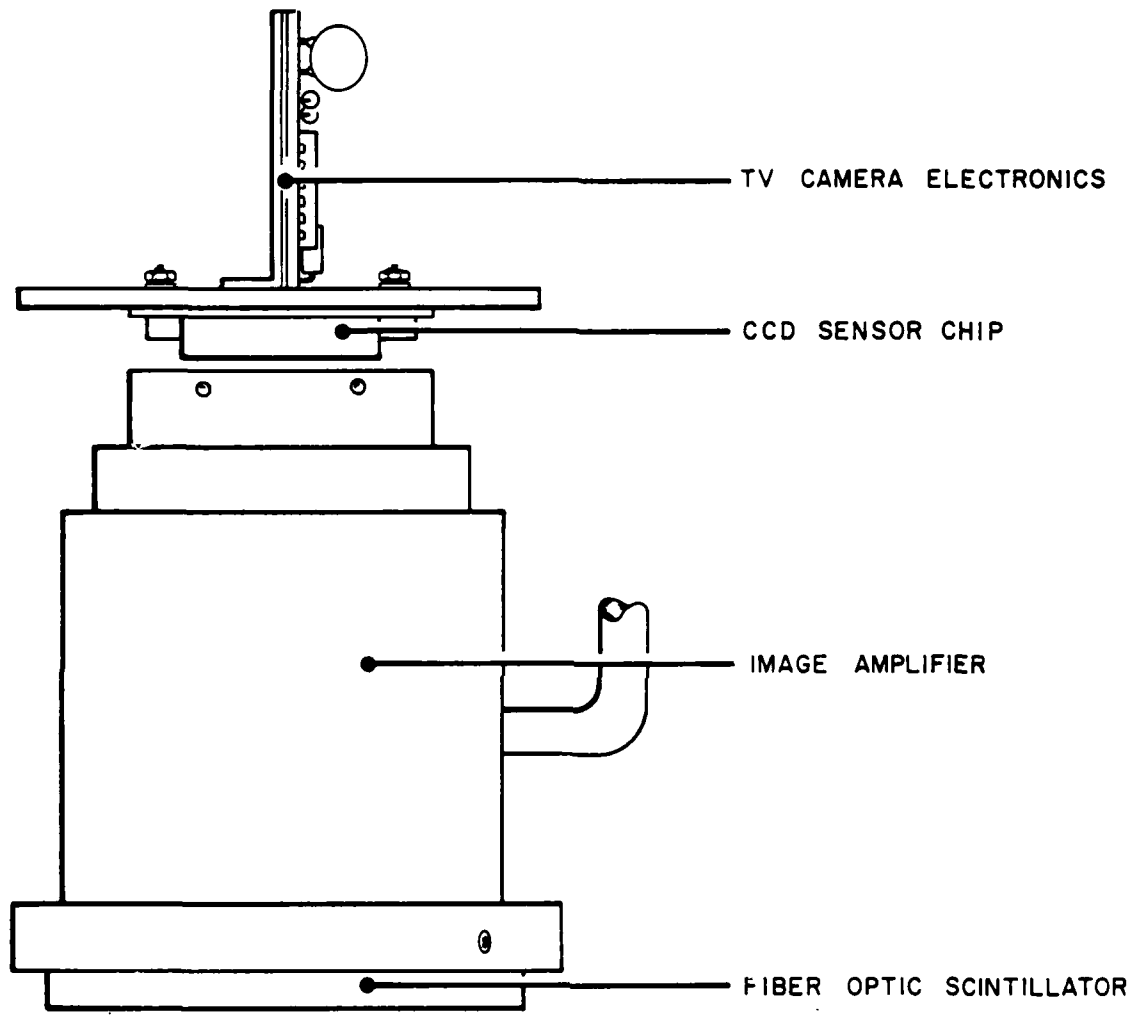


Figure 2.11. Electronics Package



2.12. FOS System Components

are approximately 25 mm (1 in.) square. These screens are made from 15 μm (0.0006 in.) diameter glass fibers with cladding of a different index of refraction. Both surfaces are optically polished and one surface is coated with a 1.5 μm (0.00006 in.) layer of aluminum for total light reflection. A second generation image intensifier is used to bring the scintillation image up to a 5 foot-lambert brightness level. The automatic gain control circuit operates the high voltage potential of the image intensifier tube to control the gain from 10 to 10,000 automatically. The TV camera is a charged coupled device (CCD) with 488 by 380 active scan lines.

2.4.2 Performance of the FOS System. For the test of the FOS system, the 25 x 25 x 2 mm scintillator plate was installed in the FOS system. A micro-focus X-ray source, a Quantex image digitizer and processor, and a TV monitor were used as support equipment. A human hand phantom and an X-ray resolution target were imaged by the FOS system in this test.

Figure 2.13 is an unprocessed image of the joint between the second and third phalanges of the little finger in the human hand phantom. The picture was taken directly from the TV monitor which was the output for the test system. Trabecular patterns can be discerned within the bone in this picture. The mottle across the image is believed to be due to the scintillation of the individual fibers in the FOS. This image was made using 34.8 kVp and 1.8 mA, an indication of superb sensitivity.

Figure 2.14 is the electronically processed image of Figure 2.13. Note the more clearly defined edges and trabecular detail as well as the improved contrast. This image was obtained in a few seconds by selecting the proper parameters on the Quantex image processor. The mottle in the image has become less noticeable, but there is a slight graininess to the image.

Figure 2.15 is the processed image of a resolution target which was placed as close to the fiber optic scintillator as was physically possible. The apparent resolving power of the system seems to be about 10 or 12 line pairs per millimeter, very good resolution for a fluoroscopic system of such high sensitivity.

2.5 Conclusions to Work Summary

The design objectives of this effort were to construct a radiographic viewing system with the following attributes:



Figure 2.13. Unprocessed Image



Figure 2.14. Processed Image

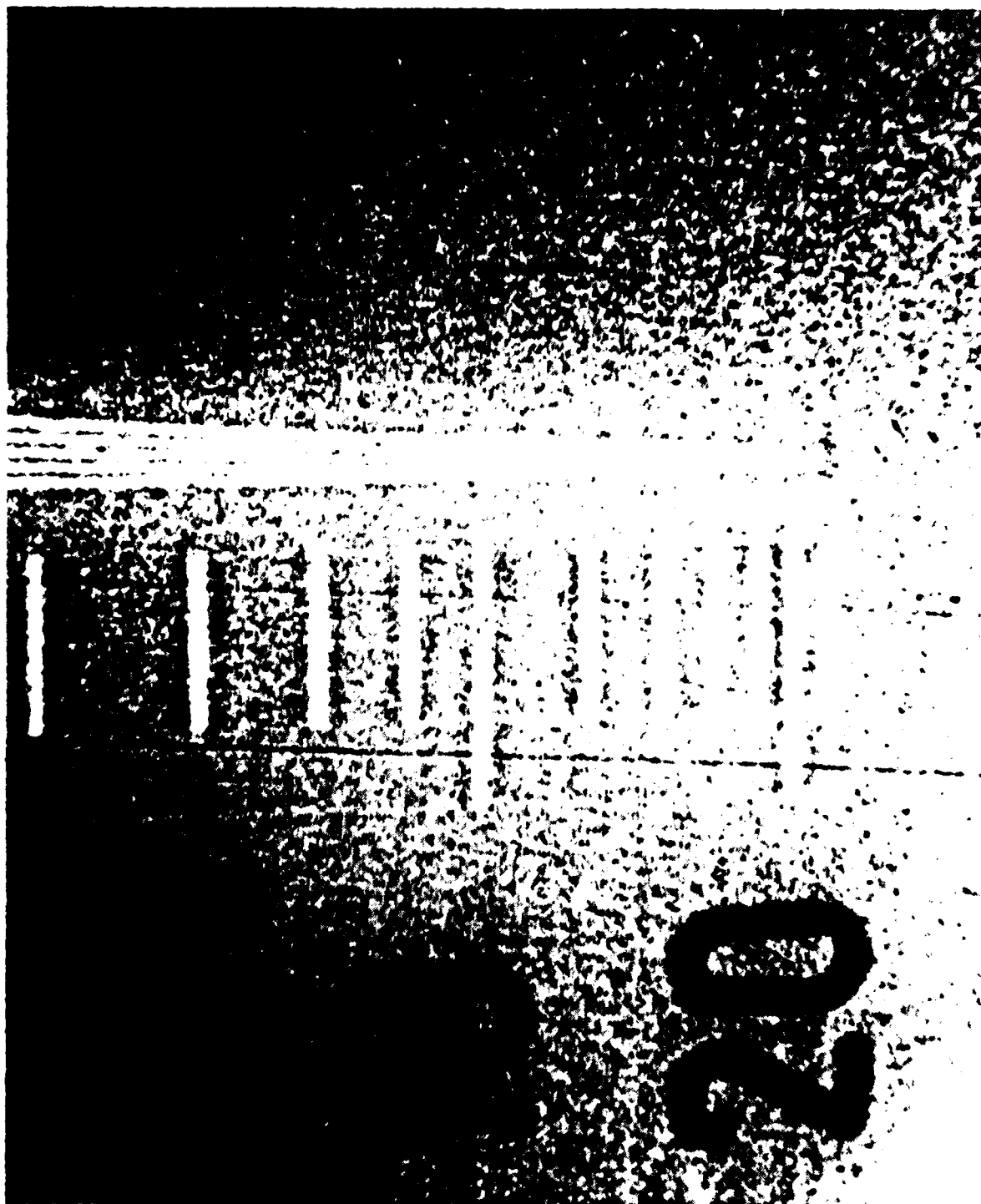


Figure 2.15. Resolution Target

- a. Compact
- b. Lightweight
- c. Rugged
- d. Good Resolution
- e. Good Sensitivity
- f. Digital Imaging

The system which was designed, constructed, and tested under this effort met each of the design objectives as follows:

- a. Compact - The sensor housing is 155 mm (6.1 in) long by 89 mm (3.5 in.) in diameter and the electronics package is 305 mm (12 in.) by 320 mm (12.5 in.) by 110 mm (4.3 in.) tall.
- b. Lightweight - Sensor weighs approximately 1 kg, (2 lbs.) and the electronics package weighs approximately 7 kg (15 lbs.).
- c. Rugged - All sensor elements are proximity focused and, therefore, in direct contact with one another and are completely enclosed in a strong aluminum housing.
- d. Good Resolution - The system displayed a resolution of approximately 10 lp/mm. This compares with 2 lp/mm for a typical fluoroscopic system and 4 lp/mm for a typical screen/film combination.
- e. Good Sensitivity - The system imaged bones of the little finger with approximately 35 kVp and 0.3 mAs. This is about an order of magnitude more sensitive than current fluoroscopic systems.
- f. Digital Imaging - The system's CCD detector allows easy conversion of analog image data to digital form.

The image area of this prototype was 25 mm x 25 mm (1 in. x 1 in.). The volume and weight will increase for a larger area, but it is anticipated that the size and weight of a FOS radiographic sensor will be smaller and will weigh less than a fluoroscopic sensor with the same image format.

SECTION 3. RELATED RESEARCH TOPICS

3.1 Digital Image Processing

A major advantage of digital radiographic images is the ability to use a computer to control the image display. This control, or processing, of the image allows one to optimize the visualization of desired image data. With present film techniques, the image may only be altered by ordering another exposure at different settings on the X-ray source or film processor. With digital imaging, a single exposure may be electronically manipulated in a number of different ways to yield:

- a. Subtraction;
- b. Spatial filtering;
- c. Pixel shifting;
- d. Temporal filtering;
- e. Intensity transformations;
- f. Parametric imaging; and
- g. Quantitative imaging.

The ability to control the image display to such a high degree and with merely a flick of a switch or twist of a knob will be a major factor in luring radiologists and other doctors away from the traditional film and light box which offers no image control.

3.1.1 Subtraction. Subtraction is the process by which one image is "subtracted" from another on a pixel by pixel basis. This is done by arithmetically subtracting the value of each pixel in one image from its corresponding pixel in the other image. The resulting image displays a cancellation of all features common to both images and an enhancement of all features which were different between the two images. Thus, subtraction produces a "difference" image and this difference is usually based on the parameters of depth, time, energy, or some combination of the three.

By utilizing depth dependent information, the effects of superimposed shadows can be removed or diminished. Depth subtraction was first utilized in motion tomography and is used most elegantly in computerized tomography (CT).

Time-dependent or temporal subtraction shows changes that occur over time. Most often temporal subtraction is used in conjunction with the administration of radiographic contrast agents. One or more precontrast images may then be subtracted from postcontrast images and, if no unwanted changes have occurred between the two, the processed image will show only the location of

the contrast medium with all other details cancelled out. This technique is used in Digital Subtraction Angiography (DSA).

Energy subtraction is based on taking an image using one energy, or wavelength, of X-ray photons and then another image at a second energy. These two images are then subtracted, yielding an image which displays the differences in the attenuation of the two energy levels of X-rays. As X-ray energy increases, the attenuation of X-ray photons will drop more rapidly in material such as bone or iodine than in material such as fat or water. This physical characteristic allows energy subtraction to be used to selectively remove certain materials from the image. Thus, energy subtraction allows soft-tissue cancellation yielding an image of only bone and iodine and it allows bone cancellation yielding an image of only soft tissue and iodine.

3.1.2 Spatial Filtering. Spatial filtering is a method of selectively enhancing or diminishing specific spatial frequency components in an image. Edges or boundaries in an image contain a large component of high-spatial-frequency information. The sharper the edge, the higher the frequencies it will contain. Thus, edge enhancement may be done by amplifying high frequencies and attenuating low frequencies in the image. The converse of edge enhancement is called smoothing and may be done by amplifying low frequencies and attenuating high frequencies.

3.1.3 Pixel Shifting. Pixel shifting, as the name implies, is a class of image processing operations where pixels, or picture elements, are moved from one location to another. This allows the image to be rotated, translated, magnified, or minified. Pixel shifting has been used in conjunction with temporal subtraction to compensate for motion which occurred between the pre-contrast and postcontrast images.

3.1.4 Temporal Filtering. Similar to spatial filtering, temporal filtering selectively attenuates either high or low temporal frequencies. In spatial filtering, the processed pixels are imaged at the same time but in different spatial locations. In temporal filtering, the processed pixels are imaged at the same spatial location but at different times. Temporal subtraction is a type of temporal filtering and so is image integration (addition) which is the process of arithmetically adding together images on a pixel by pixel basis. Image noise, especially quantum mottle, is reduced by the temporal integration of images.

3.1.5 Intensity Transformations. Another set of image processing operations, intensity transformations involve the alterations of the intensity of each image pixel based on a defined formula. Two examples familiar to radiologists are the "window" and "level" controls found on CT displays. The window setting multiplies the intensity of each pixel by a constant, thus increasing or decreasing the contrast, while the level control adds or subtracts a fixed value from each pixel, thus increasing or decreasing the brightness of the image. These two controls correspond to the contrast and brightness control knobs on a common TV. Much more complex intensity transformations are available for digital images. For instance, log conversion replaces each pixel value by its natural log, thus reducing the dynamic range of the image. Gamma correction is an operation where the value of each pixel is replaced by another value, defined by a curve, to give a straight line on the energy-density (or H-D) curve of the image. Histogram equalization is an operation that yields a final image which has equal numbers of pixels at each gray scale level, thus utilizing the dynamic range of the display to its fullest extent.

3.1.6 Parametric Imaging. In parametric imaging, each pixel value represents an estimate of a desired parameter for that pixel's location. Parameters which have been used include: time to peak enhancement, mean transit time, maximum pixel attenuation, integrated attenuation change, and local volume of distribution. Parametric imaging has been used primarily in nuclear medicine to display information about the dynamics of contrast kinetics. Parametric imaging has also been used to distinguish transplant kidney rejection and acute tubular necrosis by measuring the attenuation levels at relevant pixels as a function of time.

3.1.7 Quantitative Imaging. Since image data are in digital format, quantitative information may be easily extracted from the image by the computer. For instance, automated boundary recognition algorithms have been developed for tracing the outlines of blood vessels in order to provide quantitative estimates of narrowing. Another boundary detection algorithm has been used in the determination of ejection fraction and regional wall motion of the left ventricle of the heart from intravenous DSA images.

3.2 Optical Data Storage (ODS)

Since the FOS radiographic viewing system initially yields an electronically digitized image, it would be most convenient to store the images in that form. A digitized image contains a great many bits of information. For example, a medium resolution image of 512 x 512 pixels (or picture elements) x 256 gray levels (8 bits) contains 2 million bits of information and a high resolution image of 1024 x 1024 pixels x 256 gray levels contains 8 million bits of information. This high information content requires a storage medium with equally high capacity. A good candidate for the storage of these images seems to be optical data storage (ODS).

ODS is the technology used to produce laser video-discs. Lasers are used to burn very small holes ($5\ \mu\text{m}$ in diameter) in the metallic coating of a film base. Once the information is stored it cannot be erased for reuse of the medium and this makes it perfect for the archival storage of medical records. Optical storage is more compact than magnetic storage by more than an order of magnitude and the cost of optical storage is less than 5¢ per megabyte compared with \$3 per megabyte for magnetic storage. A credit-card size ODS with a storage strip on one side will currently hold 16 million bits of information (two high resolution pictures). With strips on two sides it would hold four pictures and, in a few years, when the $5\ \mu\text{m}$ holes are reduced to $2.5\ \mu\text{m}$ holes, the information capacity will double again. ODS discs and tapes provide greater capacities for a central storage file. A 30 cm ODS disc is currently capable of storing 2 gigabits of data on one side (or 250 high resolution pictures). An ODS tape 2,400 feet long and 70 mm wide can now store 400 gigabits of information (or 50,000 high resolution pictures).

ODS technology has only recently been made commercially available for general computer usage. It is expected that cost will decline while technical performance and data capacity increase over the next few years.

SECTION 4. GENERAL CONCLUSIONS AND RECOMMENDATIONS

The scope-of-work for this contract required the following:

- a. A study of $\text{CaF}_2(\text{Eu})$ crystals;
- b. A 16 mm fiber optic scintillator (FOS) shall be assembled from 0.1 mm fibers;
- c. Techniques for the manufacture of fine fibers and larger FOS screens shall be studied; and
- d. A report documenting the above shall be written.

In the performance of this contract, the following were completed:

- a. Several large crystals, including $\text{NaI}(\text{Th})$ and $\text{CaF}_2(\text{Eu})$, were tested and studied;
- b. A 25 mm FOS screen was assembled from 0.015 mm fibers;
- c. Techniques for the manufacture of finer fibers and larger FOS screens were studied; and
- d. This report is a document of the above.

In addition to fulfilling the scope-of-work of this contract, a small scale FOS radiographic viewing system was designed, constructed, and tested. The design objectives were to build a system which was compact, lightweight, and rugged with good resolution, sensitivity, and a digital image. As can be seen in Section 2.5, the FOS radiographic viewing system met each of these design objectives. The constructed system was a prototype with a viewing area of only one square inch, but the results of this effort have been very encouraging and indicate that it would be feasible to build a larger system based on the same design concepts. It is, therefore, recommended that a prototype of a field system with a viewing area of 200 mm x 250 mm (8 in. x 10 in.) be designed, constructed, and tested.

BIBLIOGRAPHY

Altura, Burton M., Ph.D., Lefer, Allan M., Ph.D., and Schumer, William, M.D., editors. Handbook of Shock and Trauma, Vol. 1. New York: Raven Press, 1983.

Anon., Harshaw Scintillation Phosphors, Third Edition, The Harshaw Chemical Co., Solon, Ohio, 1978.

Anon., Radiography in Modern Industry, Fourth Edition, Eastman Kodak Co., Rochester, 1980.

Anon., "Scintillators for the Physical Sciences," Brochure No. 126P, Nuclear Enterprises, Ltd., Sighthill, Edinburgh, Scotland, 1980.

Arndt, U. W. "X-Ray Television Area Detectors," Nucl. Instruments and Methods, 201, 13-20, (1982).

Berger, H. "Recent Developments in Radiography," Advanced NDE Technology, Report IGM 82-000-059, J.F. Bussiere, editor, Industrial Materials Research Institute, National Research Council of Canada, Boucherville, Quebec, pp 111-119 (1982)

Berns, Michael W. "Viewpoint: Lasers in Biomedicine," Laser Focus, June 1983.

Birks, J.B. Scintillation Counters, McGraw-Hill, New York, 1953.

Birks, J.B. Theory and Practice of Scintillation Counting, Pergamon Press, London, 1964.

Boone, W. B., Schlipper, F., and Kinchen, B., "A New Second Generation Real Time Imaging System," Qualtest-2 Conference Proceedings, p 13-1 to 13-6, Dallas, Oct. 25-27, 1983.

Borenstein, S.R. and Strand, R.C. "Scintillating Optical Fibers for Fine Grained Hodoscopes," IEEE Trans. Nuclear Science, NS-29, No. 1, 402-404 (1982).

Bril, A. and Klasens, H.A. "Intrinsic Efficiencies of Phosphors Under Cathod-Ray Excitation," Philips Research Reports, 7, 401-420 (1952).

Brody, William R., M.D., Ph.D.; Digital Radiography. New York: Raven Press, 1984.

Buchanan, R.A. "An Improved X-Ray Intensifying Screen," IEEE Trans. Nuclear Science, NS-19, No. 1, 81-86 (1971).

Cameron, John R. and Skofronick, James G. Medical Physics. New York: John Wiley and Sons, 1978.

Cameron, J.R., Suntharalingam, N., and Kenney, G.N., Thermoluminescent Dosimetry, University of Wisconsin Press, Madison, 1968.

Carnall, E. and Perlman, D. "Transparent Gd₂O₃ Ceramics and Phosphors," Materials Research Bull., 7, 647-654 (1972).

Catura, R.C. and Smithson, R.C. "Single Photon X-Ray Detection with a CCD Image Sensor," Rev. Scientific Instr., 50, No. 2, 219-220 (1979).

Chalmeton, V. "Microchannel X-Ray Image Intensifier," ASTM STP 716, pp 66-89, 1980.

Chandra, Ramesh, Ph.D. Introductory Physics of Nuclear Medicine. Philadelphia, Pa: Lea and Febiger, 1982.

Chesney, D. Noreen and Chesney, Muriel O. Radiographic Imaging. Blackwell Scientific Publications: London, 1981.

Christensen, Edward E., M.D.; Curry, Thomas S., III, M.D.; and Dowdey, James E., Ph.D. An Introduction to the Physics of Diagnostic Radiology. Philadelphia, Pa: Lea and Febiger, 1978.

Coulam, Craig M., M.D., Ph.D.; Erickson, Jon J., Ph.D.; Rollo, F. David, M.D., Ph.D.; and James, A. Everette, Jr., Sc.M., J. D., M.D.; editors. The Physical Basis of Medical Imaging. New York: Appleton - Century - Crofts, 1981.

Cullinan, John E. and Cullinan, Angeline M. Illustrated Guide to X-Ray Technics. Philadelphia, Pa: J. B. Lippincott Company, 1980.

Curran, S.C. Luminescence and the Scintillation Counter, Academic Press, New York, 1953.

de Poorter, J.A. and Bril, A., "Absolute X-Ray Efficiencies of Some Phosphors," J. Electrochemical Soc., No. 7, 1086-1088 (1975).

Dwyer, Samuel J., III, Chairman/Editor. SPIE, Vol. 418, 2nd International Conference and Workshop on Picture Archiving and Communications Systems (PACS II) for Medical Applications (May 22-25, 1983, K.C. Mo.) Bellingham Wn: SPIE -The International Society for Optical Engineering, 1983.

Dyson, N.A., M.A., Ph.D. An Introduction to Nuclear Physics, With Applications in Medicine and Biology. Chichester: Ellis Horwood Limited, 1981.

Ely, R.V., Microfocal Radiography, New York, Academic Press, 1980.

Emigh, C.R. "Radiation and Particle Physics," Section 1, Non-destructive Testing Handbook on Radiography and Radiation Testing, ANST, Columbus, 1982.

Epperson, D. "X-Ray and Ultrasonic NDE of Composite Rocket Motor Nozzles," Radiography in Aerospace, Aircraft and Nuclear Industries, ASNT, Topical Conference, abstract, July 28-30, 1981.

Evans, R.D. The Atomic Nucleus, McGraw-Hill, New York, 1955.

Fishman, G.J. "Images of Single X-Ray Photons from X-Ray Phosphor Screens," Rev. Scientific Instr., 52, no. 8, 143-1147 (1981).

Fullerton, Gary D., Hans, Arthur G., Properzio, William S., and Mulvaney, James A., editors. SPIE, Vol. 347, Application of Optical Instrumentation in Medicine X. (May 9-12, 1982, New Orleans, La.): Bellingham, Wn: SPIE - The International Society for Optical Engineering, 1982.

Gamble, R.C., Baldeschweiler, J.D. and Griffin, C.E. "Linear Position-Sensitive X-Ray Detector Incorporating a Self-Scanned Photodiode Array," Rev. Scientific Instr., 50, No. 11, 1416-1420 (1979).

Garrett, D.A. and Bracher, D.A., editors (ASTM Special Technical publication 716). Real-Time Radiologic Imaging: Medical and Industrial Application. Symposium at Gaithersburg, Md., 8-10 May 1978. Pa: American Society for Testing and Materials, 1980.

Garrett, D.A. and Bracher, D.A. editors, "Real-Time Radiologic Imaging: Medical and Industrial Applications," ASTM STP 716, American Society for Testing and Materials, Philadelphia, 1980.

Glocker, V.R. "Die Abhangigkeit der Reichweite der Elektronen von ihrer Energie," Z. Naturforsch., 3A, 129, 147-151 (1948).

Gray, Henry, F.R.S., Anatomy, Descriptive and Surgical. New York: Bounty Books, Crown publishers, Inc., 1977.

Grum, F., Costa, L.F. and Donovan, J.L. "Measured Light-Emission Efficiency and Quantum Yield for X-Ray Screens and Phosphors," J. Optical Soc. Americas, 59, N9. 7, 848-850 (1969).

Gruner, S.M., Milch, J.R. and Reynolds, G.T. "Evaluation of Area Photon Detectors by a Method Based on Detective Quantum Efficiency (DQE)," IEEE Trans. Nuclear Science, NS-25, No. 1, 562-565 (1978).

Gruner, S.M., Milch, J.R. and Reynolds, G.T. "Slow-Scan Silicon-Intensified Target-TV X-Ray Detector for Quantitative Recording of Weak X-Ray Images," Rev. Scientific Instr., No. 11, 1770-1778 (1982).

Gruner, S.M., Milch, J.R. and Reynolds, G.T. "Survey of Two-Dimensional Electro-Optical X-Ray Detectors," Nucl. Instruments and Methods, 195, 287-297 (1982).

Halmshaw, R., editor, Physics of Industrial Radiology, Heywood, London, 1966.

Hay, G.A., "X-Ray Imaging," J. Phys. E: Scientific Instr., 11, 377-386 (1978).

Herz, R.H., The Photographic Action of Ionizing Radiations, Wiley-Interscience, New York, 1969.

Hopwood, R.K. "Design Considerations for a Solid-State Image Sensing System," Proc. Soc. Photo-Optical Instr. Eng., 230, 72-82 (1980).

Jensen, J. Trygve, Ed.D.; Physics for the Health Professions. New York; John Wiley and Sons, 1982.

Keats, Theodore E., M.D. Emergency Radiology. Chicago: Year Book Medical Publishers, Inc., 1984.

Kittel, Charles. Elementary Solid State Physics: A Short Course. New York and London: John Wiley and Sons, Inc., 1962.

Knoll, G.F. Radiation Detection and Measurement, J. Wiley & Sons, New York, 1979.

Leverenz, H.W. An Introduction to Luminescence of Solids, J. Wiley & Sons, New York, 1950.

Logan, Wende Westinghouse, M.D., editors. Reduced Dose Mammography. New York: MASSON Publishing USA, Inc., 1979.

Ludwig, G.W. "X-Ray Efficiency of Phosphor Powders," J. Electrochemical Soc., 118, No. 7, 1152-1159 (1971).

Lutz, S.S., Franks, L.A., Fluornoy, J.M. and Lyons, P.B. "Scintillators for Fiber Optics: System Sensitivity and Bandwidth as a Function of their Length," Proc. Soc. Photo-Optical Instr. Eng., 296, 156-163 (1981).

McGinnis, J. "X-Ray Sensitive Photodiode Array," Industrial Res. and Dev., 143-146 (March, 1980).

McMaster, R.C., editor, Nondestructive Testing Handbook, American Society for Nondestructive Testing, Columbus, 1959.

Moore, B.M and Walker, A. "Light Output and X-Ray Attenuation Measurements for Some Commercial Intensifying Screens," Radiology, 28, 767-774 (1978).

Moore, B.M., Parker, R.P. and Pullan, B.R., editors. Physical Aspects of Medical Imaging (proceedings of a meeting held at the University of Manchester, 25-27 June, 1980). New York: John Wiley and Sons, 1981.

Mott, N.F. and Gurney, R.W. Electronic Processes in Ionic Crystals, Oxford University Press, Oxford, 1940.

Motz, J.W. and Danos, M. "Image Information Content and Patient Exposure," Medical Physics, 5, No. 1 8-22 (1978).

Noz, Marilyn E., Ph.D and Maguire, Gerald Q., Jr., Radiation Protection in the Radiology and Health Sciences. Philadelphia, PA; Lea and Febiger, 1979.

Nudelman, S., Fisher, H.D., Frost, M.M., Capp, M.P. and Ovitt, T.W. "A Study of Photoelectronic-Digital Radiology - Part I: The Photoelectronic-Digital Radiology Department," Proc. IEEE, 70, No. 7, 700-707 (1982).

Nudelman, S., Healy, J. and Capp, M.P. "A Study of Photoelectronic-Digital Radiology - Part II: Cost Analysis of a Photoelectronic-Digital Versus Film-Based System for Radiology," Proc. IEEE, 70, No. 7, 708-714 (1982).

Nudelman, S., Roehrig, H. and Capp, M.P. "A Study of Photoelectronic-Digital Radiology - Part III: Image Acquisition Components and System Design," Proc. IEEE, 70, No. 7, 715-727 (1982).

Peckerar, M.C., McCann, D.H. and Yu, L. "X-Ray Imaging with a Charge-Coupled Device Fabricated on a High Resistivity Silicon Substrate," Appl. Physics Lett., 39, No. 1, 55-57 (1981).

Price, Ronald R. Ph.D., Rollo, F. David, M.D., Ph.D., Monahan, W. Gordon, Ph.D., and James A. Everette, Jr., S.C.M., J.D., M.D., editors. Digital Radiography: A Focus on Clinical Utility. New York: Grune and Stratton, 1982.

Rimkus, D. and Baily, N.A. "Quantum Noise in Detectors," Medical Physics, 10, No. 4, 470-471 (1983).

Roeske, F., Rotter, M.D., Calavan, P.M. and Lutz, S.S. "Radiation-to-Light Converters for Nuclear Environments: Near-Infrared Emitters," Proc. Soc. Photo-Optical Instr. Eng., 296, 170-176 (1981).

Rose, A. "The Sensitivity of the Human Eye on an Absolute Scale," J. Optical Soc. Amer., 38, 196-208 (1948).

Rosell, F.A. "The Limiting Resolution of Low-Light Level Imaging Sensors," in Photoelectronic Imaging Devices, L.M. Biberman and S. Nudelman, editors, Plenum Press, New York, 1971, pp 308-329.

Schagen, P. "X-Ray Imaging Tubes," NDT International, 14, No. 1, 9-14 (1981).

Seitz, F. Modern Theory of Solids, McGraw-Hill, New York, 1940.

Spiller, Eberhard, Chairman/Editor. SPIE, Volume 316, High Resolution Soft X-Ray Optics (November 18-20, 1981, Brookhaven, N.Y.). Bellingham, Wn: SPIE -The International Society for Optical Engineering, 1982.

Spowart, A.R. "Energy Transfer in Cerium-Activated Silicate Glasses," J. Phys. C: Solid State Phys., 12, 3369-3374 (1979).

Spowart, A.R. "Energy Transfer in Terbium-Activated Silicate Glasses," J. Phys. C: Solid State Phys., 12, 3375-3380 (1979).

Stevens, A.L.N. and Schrama-de Pauw, A.D.M. "Vapour-Deposited CsI: Na Layers, II. Screens for Application in X-Ray Imaging Devices," Philips Research Reports, 29, 353-362 (1974).

Strum, R.E. and Morgan, R.H. "Screen Intensification Systems and Their Limitations," Amer. J. Roentgenology and Radium Therapy, 62, No. 5, 617-637 (1949).

Van Der Plaats, G.J., Radiologist. Medical X-Ray Techniques in Diagnostic Radiology. London: Martinus Nijhoff Publishers, 1980.

Van Der Plaats, G. J. and Vijlbrief, assistant. Medical X-Ray Techniques in Diagnostic Radiology. The Hague/Boston/London: Martinus Nijheff, 1980.

Venema, H.W. "X-Ray Absorption, Speed and Luminescent Efficiency of Rare Earth and Other Intensifying Screens," Radiology, 130, 765-771 (1979).

Wang, S.P., Laudi, O., Lucks, H., Wickersheim, K.A. and Buchanan, R.A. "X-Ray Image Intensifier Tubes Using Rare Earth Oxysulfide Phosphors," IEEE Trans. Nuclear Science, NS-17, No. 1, 49-56 (1970).

Whalen, Joseph P., M.D. and Balter, Stephen, Ph.D. Radiation Risks in Medical Imaging. Chicago and London: Year Book Medical Publishers, Inc., 1984.

Wickersheim, K.A., Alves, R.V. and Buchanan, R.A. "Rare Earth Oxysulfide X-Ray Phosphors," IEEE Trans. Nuclear Science, NS-17, No. 1, 57-60 (1970).

Yang, M.J., Gabriel, R., Kinnison, W.W., Matis, H.S. and Anderson, H.L. "Fiber-Optics Light Guides for Thin Scintillators," Nucl. Instruments and Methods, 185 115-117 (1981).

Yin, L.I., Trombka, J.I. and Seltzer, S.M. "New Position-Sensitive Hard X-Ray Spectrometer," Rev. Scientific Instr., 51, No. 6, 844-845 (1981).

Young, Stuart W., M.D., Nuclear Magnetic Resonance Imaging. New York: Raven Press, 1984.

MAGAZINES

Applied Radiology, Los Angeles: Barrington Publications, Inc.

Perinatology Neonatology, Los Angeles: Barrington Publications, Inc.

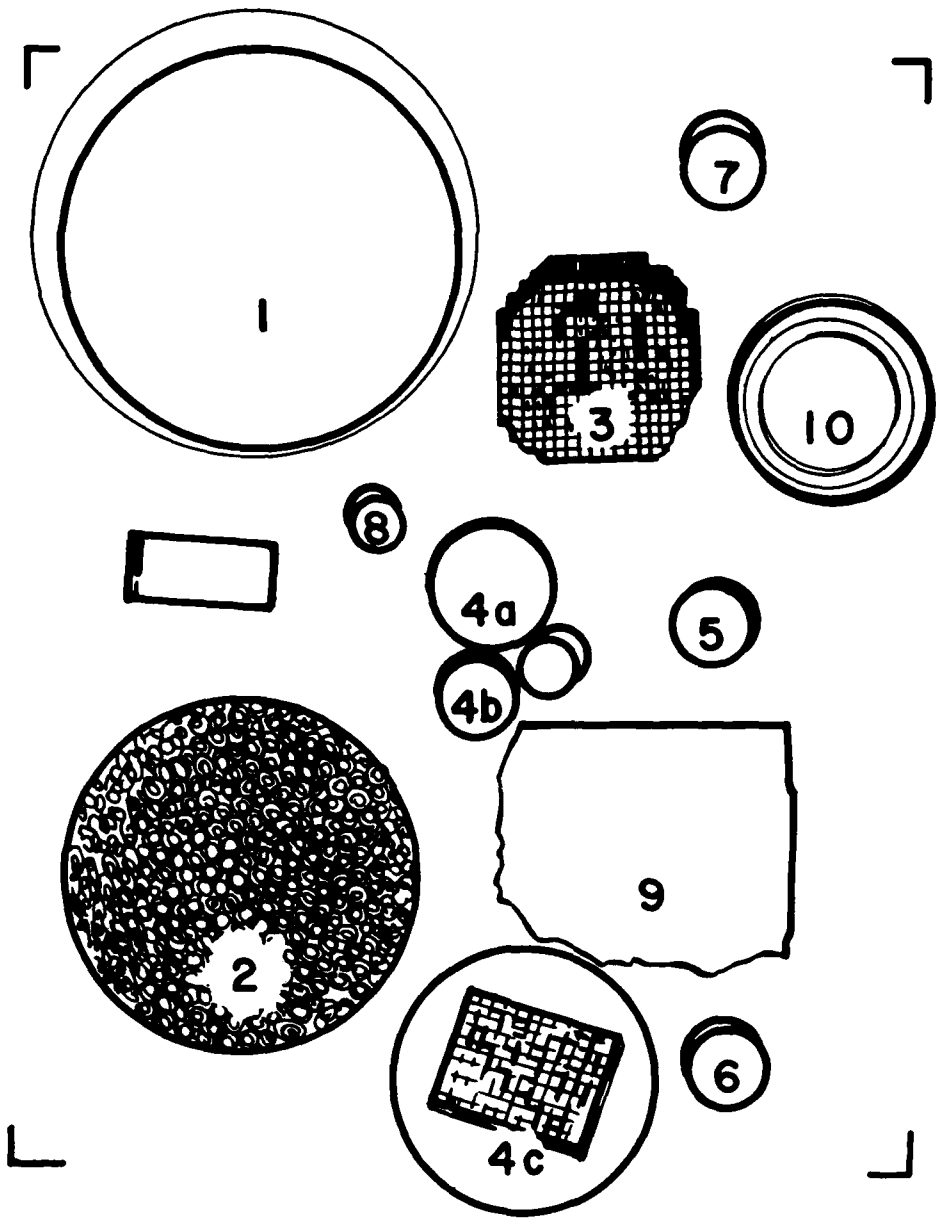
Vascular Diagnosis and Therapy, Los Angeles: Barrington Publications, Inc.

CVP, Los Angeles: Barrington Publications, Inc.

Medical World News, Houston: HEI Publishing, Inc.

LITERATURE CITED

1. J.B. Birks, Scintillation Counters, McGraw-Hill, New York, 1953.
2. H.W. Leverenz, An Introduction to Luminescence of Solids, J. Wiley, New York, 1950.
3. R.H. Herz, The Photographic Action of Ionizing Radiations, Wiley-Interscience, New York, 1969.
4. G.F. Knoll, Radiation Detection and Measurement, J. Wiley, New York, 1979.
5. R. Halmshaw, editor, Physics of Industrial Radiology, Heywood Books, London, 1966, pages 119-120.
6. K.A. Wickersheim, R.V. Alves and R.A. Buchanan, "Rare Earth Oxysulfide X-Ray Phosphors," IEEE Trans. Nuclear Science, NS-17, No. 1, 57-60 (Feb., 1970).
7. A.R. Spowart, "Energy Transfer in Cerium-Activated Silicate Glasses," J. Phys. C: Solid State Phys., 12, 3369-3374 (1979).
8. A.R. Spowart, "Energy Transfer in Terbium-Activated Silicate Glasses," J. Phys. C: Solid State Phys., 12, 3375-3380 (1979).
9. R.D. Evans, The Atomic Nucleus, McGraw-Hill, New York, 1955.
10. Ref. 9, page 695.
11. V.R. Glocker, "Die Abhangigkeit der Reichweite der Elektronen von ihrer Energie," Z. Naturforsch., 3A, 129, 147-151 (1948).
12. Ref. 4, pages 318-319.



LOCATION OF SAMPLES LISTED ON PAGE 18

